[AMERICAN JOURNAL OF SCIENCE, VOL. 259, DECEMBER 1961, P. 735-765]

# STABILITY RELATIONS OF GLAUCOPHANE

W. G. ERNST*

Geophysical Laboratory, Carnegie Institution of Washington.
Washington, D. C.

ABSTRACT. Stability relations have been determined for glaucophane [$oNa_2Mg_3Al_2Si_8O_{22}(OH)_2$] + excess vapor and for quartz + glaucophane + vapor using conventional hydrothermal techniques. The high-temperature stability limit of this amphibole ranges from 850°C at 175 bars vapor (= total) pressure to 868°C at 2000 bars $P_{vapor}$. Neither differential stress nor high pressures are necessary for the formation of glaucophane. The presence of excess silica lowers its high-temperature stability limit only 3°-6°C.

Unusually large enthalpy values for the reactions glaucophane → forsterite + enstatite + albite + vapor, and quartz + glaucophane → enstatite + albite + vapor (330 ± 60 and 320 ± 60 kcal/mol respectively) may be explained only in part by the change in coordination of aluminum from 6 in glaucophane to 4 in albite. The entropy of glaucophane at 864°C and 1000 bars vapor pressure is 150 ± 50 cal/deg/mol.

Optical properties of synthetic glaucophane agree well with data for natural specimens. Unit cell dimensions of the synthetic material are slightly larger than those of natural glaucophanes.

The experimental investigation indicates that glaucophane is stable over a wide range of physical conditions given appropriate chemical conditions. Bulk compositions rich in soda and magnesia and poor in lime relative to alumina should favor production of glaucophane. The rare occurrence of such chemical environments severely restricts the crystallization of glaucophane in nature.

## INTRODUCTION

In the past fifteen years glaucophane schists have been intensively studied in the Alps, California, the Caribbean area, Corsica, Indonesia, and Japan. Through clarification of the field, mineralogic, and chemical relations, such examinations have contributed greatly to an understanding of these rocks. Nevertheless, the petrogenesis of glaucophane schists is still debated. A number of geologists believe that glaucophane schists are products of relatively high pressures and low temperatures and represent a distinct metamorphic facies. Other workers contend that special chemical conditions have produced glaucophane-bearing rocks at moderate pressures and low temperatures.

Experimental investigation of glaucophane was undertaken to determine the physical and chemical parameters governing the stability of this mineral, in the hope of better understanding the larger problem concerning origin of the glaucophane schists.

## EXPERIMENTAL TECHNIQUES

Hydrothermal equipment, temperature and pressure regulators, and recorders employed in this investigation were similar to those described in another paper (Ernst, 1960); the preparation of starting material, and X-ray and optical analyses of run products were also described in that report. Charges were sealed in platinum tubes containing excess water. Stable phases were necessarily in equilibrium with vapor (fluid approaching the composition $H_2O$) for the investigated range of temperatures and pressures; thus $P_{vapor} = P_{total}$.

Phase relations were determined for two compositions, (1) $Na_2O \cdot 3MgO \cdot Al_2O_3 \cdot 8SiO_2$ + excess $H_2O$ (glaucophane + vapor), and (2) $Na_2O \cdot 3MgO \cdot$

* Present address: Department of Geology and Institute of Geophysics, University of California, Los Angeles, California.

$Al_2O_3 \cdot 10SiO_2$ + excess $H_2O$ (quartz + glaucophane + vapor = talc + albite + vapor). Starting materials were oxide mixtures, glasses of the composition $Na_2O \cdot 3MgO \cdot Al_2O_3 \cdot 8SiO_2$ and $Na_2O \cdot 3MgO \cdot Al_2O_3 \cdot 10SiO_2$ prepared by J. F. Schairer, mixtures of reagent talc and Amelia albite in the proportion $Na_2O \cdot 3MgO \cdot Al_2O_3 \cdot 10SiO_2 \cdot H_2O$, and synthetic enstatite and Amelia albite in the proportion $Na_2O \cdot 3MgO \cdot Al_2O_3 \cdot 9SiO_2$. Several batches of oxide mix and glass were ground 12-18 hours in a motor-driven boron carbide mortar (made available by A. Van Valkenburg, National Bureau of Standards) to decrease grain size and thereby increase reactivity of the charge.

Proof that the observed glaucophane reactions are reversible was obtained by decomposing synthetic glaucophane at temperatures above its high-temperature stability limit; high-temperature phase assemblages equivalent in composition to glaucophane and to quartz + glaucophane were reacted to form glaucophane within the amphibole stability field.

## DESCRIPTION OF SYNTHETIC GLAUCOPHANE

### *Determination of Amphibole Composition*

The yield of amphibole under appropriate $P_{vapor}$-T conditions ranged from less than 1 percent of the condensed assemblage to over 70 percent; yields of 10-20 percent were typical. (Several experiments in which the fluxes NaOH, NaCl, and HCl were employed resulted in increased production of amphibole.) The remainder consisted of phases of the high-temperature equivalent assemblages; for the investigated bulk compositions, these phases are metastable in the amphibole field. At a given temperature and pressure, more amphibole was obtained on long runs than on short runs, as illustrated in figure 1. Refractive indices and d values of the amphibole showed no measurable variation with the amount obtained and were independent of starting material. Optical constants for the amphibole are in good agreement with those of natural glaucophane. The relative proportions among metastable phases obtained within the amphibole field of stability were unaffected by the amount of amphibole present, and were the same as the relative proportions among these phases at temperatures in excess of the amphibole field boundary, as deduced by comparison with X-ray standards. This observation is further substantiated by micrometric analyses presented in table 2. Within limits of error of the point-counting technique, relative proportions among the metastable phases of the high-temperature assemblage are equivalent to the bulk composition, so that the amphibole likewise must be "on composition." Dehydration of the amphibole indicates a water content of $3 \pm 1$ weight percent, in reasonably good agreement with the theoretical value for glaucophane of 2.3 weight percent $H_2O$. From all the above data, the synthetic amphibole produced in this study is deduced to have the composition of glaucophane.

### *Glaucophane Optical Data*

Refractive indices and extinction angles of synthetic glaucophane are presented in table 3. Crystals were about 0.020-0.040 mm long and 0.001-0.003 mm in diameter. Amphibole grown over a wide temperature and pressure range showed no variation in optical properties. Glaucophane crystallized from

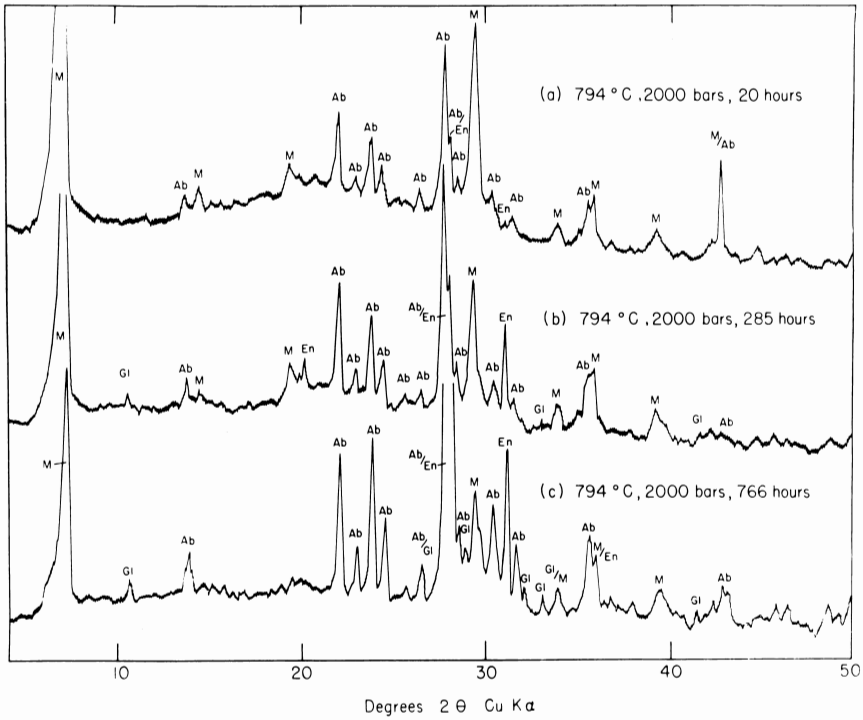


Fig. 1. Growth study of stable and metastable phases obtained for the bulk composition $Na_2O \cdot 3MgO \cdot Al_2O_3 \cdot 8SiO_2$ + excess water within the stability field of glaucophane. Sodic montmorillonite is presumed to be metastable because glaucophane and the high-temperature assemblage of equivalent bulk composition grow at its expense. Positions of X-ray diffraction peaks for sodic montmorillonite indicate partial dehydration. Abbreviations used throughout this paper are listed in table 1.

the breakdown products (high-temperature assemblage of bulk compositions equivalent to glaucophane and quartz + glaucophane) is indistinguishable from that synthesized from an oxide mixture or from glass. The refractive indices of synthetic glaucophane lie between those of an iron-poor natural specimen from Zermatt, Switzerland (Kunitz, 1930, p. 198), and values of a theoretical end member extrapolated by Winchell and Winchell (1951, p. 441) using natural members of the glaucophane-riebeckite series.

TABLE 1

Abbreviations used in this paper

Ab = albite
Cr = cristobalite
En = enstatite
Fo = forsterite
Gl = glaucophane
L = liquid
M = sodic montmorillonite
Pr = protoenstatite
Q = quartz
Tc = talc
Tr = tridymite
V = vapor
( ) = enclose phases interpreted as metastable
? = presence not definitely established
mix = oxide mixture
condensed starting material prefix:
Gl = $Na_2O \cdot 3MgO \cdot Al_2O_3 \cdot 8SiO_2$
Q + Gl = $Na_2O \cdot 3MgO \cdot Al_2O_3 \cdot 10SiO_2$

TABLE 2

Micrometric analyses of condensed run products within the amphibole field of stability for the bulk compositions $Na_2O \cdot 3MgO \cdot Al_2O_3 \cdot 8SiO_2 + H_2O$ and $Na_2O \cdot 3MgO \cdot Al_2O_3 \cdot 10SiO_2 + H_2O$

| Condensed Starting Material | Temp. in °C | $P_{vapor}$ in bars | Duration in hours | Relative Modal Proportions of Metastable Phases Fo | En | Ab | Q | Total Vol. percent Gl |
|---|---|---|---|---|---|---|---|---|
| Gl mix | 852 | 175 | 500 | 15 | 10 | 75 | 0 | 14 |
| Gl mix | 841 | 300 | 232 | 16 | 11 | 73 | 0 | 11 |
| Gl mix | 830 | 305 | 246 | 13 | 12 | 75 | 0 | 7 |
| Gl mix | 826 | 1200 | 142 | 16 | 12 | 72 | 0 | 15 |
| Gl glass | 760 | 2000 | 221 | 14 | 10 | 76 | 0 | 22 |
| Computed proportions for the bulk composition $Na_2O \cdot 3MgO \cdot Al_2O_3 \cdot 8SiO_2$ ..... | | | | 15.8 | 11.4 | 72.8 | 0.0 | |
| Q + Gl mix | 814 | 505 | 280 | 0 | 32 | 62 | 6 | 7 |
| Computed proportions for the bulk composition $Na_2O \cdot 3MgO \cdot Al_2O_3 \cdot 10SiO_2$ .... | | | | 0.0 | 29.6 | 63.3 | 7.1 | |

(1050-1250 points counted for each sample)

TABLE 3

Optical properties of synthetic and natural glaucophane

| Condensed Starting Material | Temp. in °C | $P_{vapor}$ in bars | Duration in hours | $N_x$ | $N_z$ | Extinction Angle $Z \wedge c$ in ° |
|---|---|---|---|---|---|---|
| Gl mix | 862 | 1875 | 6 | 1.594 | 1.620 | 9 |
| Gl mix | 857 | 1690 | 10 | 1.595 | 1.620 | 10 |
| Fo + En + Ab | 850 | 825 | 185 | 1.596 | 1.620 | 9 |
| Gl mix | 850 | 825 | 185 | 1.596 | 1.620 | 7 |
| Gl mix | 840 | 825 | 168 | 1.596 | 1.619 | 8 |
| Gl mix | 830 | 175 | 500 | 1.596 | 1.620 | 9 |
| Gl glass | 815 | 1000 | 1920 | 1.595 | 1.621 | 10 |
| Fo + En + Ab | 794 | 2000 | 776 | 1.595 | 1.620 | 8 |
| Gl mix | 794 | 2000 | 776 | 1.594 | 1.620 | 10 |
| Gl mix | 794 | 2000 | 285 | 1.596 | 1.619 | 6 |
| Fo + En + Ab | 776 | 800 | 280 | 1.594 | 1.620 | 8 |
| Gl mix | 652 | 2500 | 870 | 1.594 | 1.620 | 11 |
| En + Ab + Q + Gl | 852 | 250 | 991 | 1.594 | 1.620 | 11 |
| Q + Gl mix | 836 | 1730 | 38 | 1.596 | 1.620 | 14 |
| Tc + Ab | 815 | 1000 | 1920 | 1.595 | 1.621 | 10 |
| En + Ab + Q | 792 | 1500 | 480 | 1.595 | 1.620 | 14 |
| Tc + Ab | 789 | 1510 | 474 | 1.594 | 1.618 | 6 |
| En + Ab + Q | 745 | 2000 | 332 | 1.594 | 1.621 | 12 |
| Q + Gl mix | 745 | 2000 | 332 | 1.594 | 1.620 | 11 |
| Q + Gl mix | 702 | 2020 | 240 | 1.594 | 1.619 | 8 |
| Winchell and Winchell (1951) projected end member .... | | | | 1.586 | 1.613 | 8 |
| Kunitz (1930) iron-poor glaucophane (~85 glaucophane, ~15 riebeckite) ..... | | | | 1.606 | 1.627 | 8 |

All measurements of synthetic material performed using white light, index oils of 0.002 interval, and corrected for temperature variation; indices of refraction considered accurate to within ± 0.003, extinction angles to within ±4°.

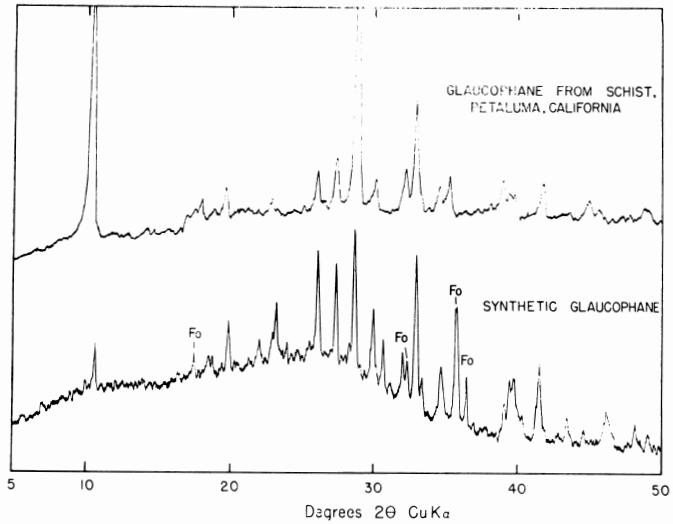


Fig. 2. X-ray diffractometer patterns for synthetic and natural glaucophane; differences in amplitudes of corresponding peaks suggest preferred orientation of the natural specimen. The synthetic material contains the additional phases forsterite and glass.

## *Glaucophane X-ray Data*

In figure 2 the X-ray diffractometer pattern of synthetic glaucophane is compared with that of a natural sample from Petaluma, California, supplied by A. Pabst, University of California. The synthetic material was indexed by comparison with synthetic magnesioriebeckite (Ernst, 1960, table 14). Five peaks were measured (see table 4) using Lake Toxaway quartz as an internal standard. From these measurements, cell dimensions and Q values were calculated. Table 5 presents d values, intensities, Q values, and $2\theta$ values for all measured diffraction peaks of synthetic glaucophane.

In table 6 lattice parameters and cell volumes of synthetic glaucophane and synthetic magnesioriebeckite are compared. The latter has a larger unit cell because the ionic radius of ferric iron exceeds that of aluminum. Some natural glaucophanes have unit cell dimensions smaller than those of the synthetic analogue; deviation of the natural material from the stochiometric pro-

TABLE 4

Averages of six measurements of X-ray diffraction peaks for synthetic glaucophane (space group C2/m)

| Reflection | $2\theta_{ave.}$* | Standard (Chart) Error of the Mean |
|---|---|---|
| 040 | 19.814 | ±0.0060 |
| 131 | 26.114 | ±0.0041 |
| 310 | 28.691 | ±0.0054 |
| 151 | 33.000 | ±0.0064 |
| $\bar{2}02$ | 35.894 | ±0.0068 |

*CuK$\alpha$ = 1.5418 Å.

TABLE 5

X-ray powder data for synthetic glaucophane (space group C2/m)

| Reflection | $2\theta_{obs}$* | $Q_{calc}$ | $\Delta Q$ | I | d in Å |
|---|---|---|---|---|---|
| 020 | 9.82 | .01245 | .00013 | 9 | 9.00 |
| 110 | 10.56 | .01425 | .00001 | 32 | 8.38 |
| $\bar{1}11$ | 18.42 | .04306 | −.00001 | 12 | 4.818 |
| 040 | 19.814 | .04981 | .00000 | 36 | 4.481 |
| 111 | 21.95 | .06100 | .00000 | 19 | 4.049 |
| $\bar{1}31$ | 23.19 | .06796 | −.00003 | 35 | 3.885 |
| 131 | 26.114 | .08591 | .00001 | 72 | 3.412 |
| 240 | 27.38 | .09434 | .00009 | 65 | 3.257 |
| 310 | 28.691 | .10331 | .00000 | 91 | 3.120 |
| 221 | 29.99 | .11271 | .00009 | 50 | 2.980 |
| $\bar{1}51$ | 30.69 | .11777 | −.00004 | 34 | 2.913 |
| 330 | 32.04 | .12821 | .00006 | 24 | 2.794 |
| 151 | 33.000 | .13572 | −.00001 | 100 | 2.714 |
| 331 | 33.40 | .13907 | .00013 | 20 | 2.683 |
| 241 | 34.76 | .15007 | −.00010 | 32 | 2.581 |
| $\bar{2}02$ | 35.894 | .15977 | .00000 | 81 | 2.502 |
| $\bar{3}51$ | 39.14 | .18888 | .00005 | 13 | 2.301 |
| 331 / 080 | 39.79 | .19292 / .19923 | —— | 25 | 2.265 |
| 261 | 41.56 | .21233 | .00059 | 50 | 2.173 |
| 202 | 43.49 | .23156 | .00061 | 15 | 2.081 |
| 351 | 44.63 | .24272 | .00017 | 9 | 2.031 |
| 242 | 48.23 | .28137 | .00044 | 16 | 1.887 |

*CuK$\alpha$ = 1.5418 Å

$\Delta Q = Q_{calc} - Q_{obs}$.

Intensities estimated from peak height.

portions $Na_2O \cdot 3MgO \cdot Al_2O_3 \cdot 8SiO_2 \cdot H_2O$, or the existence of two glaucophane polymorphs (Ernst, 1959) may account for this discrepancy.

## EXPERIMENTAL RESULTS

### *Run Data*

Tables 7 and 8 present the results of hydrothermal investigation of the bulk compositions $Na_2O \cdot 3MgO \cdot Al_2O_3 \cdot 8SiO_2$ + excess water and $Na_2O \cdot 3MgO \cdot Al_2O_3 \cdot 10SiO_2$ + excess water. Three experiments employing the bulk composition $Na_2O \cdot 3MgO \cdot Al_2O_3 \cdot 9SiO_2$ + excess water (quartz + glaucophane + vapor = enstatite + albite + vapor) are listed at the end of table 8.

TABLE 6

Unit cell dimensions of synthetic glaucophane and magnesioriebeckite (space group C2/m)

| Synthetic Glaucophane | Synthetic Magnesioriebeckite |
|---|---|
| a = 9.71 Å | a = 9.79 Å |
| b = 17.92 Å | b = 18.02 Å |
| c = 5.27 Å | c = 5.28 Å |
| $\beta$ = 102.6° | $\beta$ = 102.6° |
| cell volume = 895.4 Å$^3$ | cell volume = 908.6 Å$^3$ |

TABLE 7

Results of investigations of the composition $Na_2O \cdot 3MgO \cdot Al_2O_3 \cdot 8SiO_2$ with excess water

| Condensed Starting Material | Temp. in °C | $P_{vapor}$ in bars | Duration in hours | Condensed Run Products |
|---|---|---|---|---|
| | Curve: Fo + En + Ab + Gl + V | | | |
| mix | 840 | 175 | 500 | Gl (+Fo + En + Ab) |
| mix | 852 | 175 | 500 | Fo + En + Ab + Gl |
| Fo + En + Ab | 852 | 180 | 500 | Fo + En + Ab + Gl? |
| mix | 841 | 300 | 232 | Gl (+ Fo + En + Ab) |
| Fo + Gl + L | 856 | 302 | 402 | Fo + En + Ab + Gl |
| mix | 856 | 302 | 402 | Fo + En + Ab + Gl |
| glass | 865 | 300 | 279 | Fo + En + Ab |
| mix | 863 | 390 | 194 | Fo + En + Ab |
| mix | 847 | 500 | 283 | Gl (+ Fo + En + Ab) |
| mix | 861 | 500 | 259 | Fo + En + Ab + Gl |
| mix | 873 | 500 | 162 | Fo + En + Ab |
| Fo + En + Ab | 860 | 820 | 184 | Gl (+ Fo + En + Ab) |
| mix | 860 | 820 | 184 | Gl (+ Fo + En + Ab) |
| Fo + En + Ab + Gl | 866 | 815 | 163 | Fo + En + Ab |
| mix | 853 | 1000 | 139 | Gl (+ Fo + En + L) |
| mix | 865 | 1020 | 117 | Fo + En + Ab |
| mix | 859 | 1310 | 66 | Gl (+ Fo + En + Ab) |
| Fo + En + Ab + Gl | 862 | 1210 | 96 | Fo + En + Ab + Gl? |
| Fo + En + Ab | 862 | 1210 | 96 | Fo + En + Ab |
| glass | 871 | 1240 | 118 | Fo + En + Ab (+ L) |
| mix | 857 | 1520 | 100 | Gl (+ Fo + En + Ab) |
| mix | 867 | 1490 | 99 | Fo + En + Ab + L |
| Fo + En + Ab | 868 | 1500 | 79 | Fo + En + L |
| | Field: Gl + V | | | |
| mix | 830 | 175 | 500 | Gl (+ Fo + En + Ab) |
| mix | 820 | 240 | 2215 | Gl (+ Fo + En + Ab) |
| mix | 830 | 305 | 246 | Gl (+ Fo + En + Ab) |
| Fo + En + Ab | 835 | 295 | 473 | Gl (+ Fo + En + Ab) |
| Fo + En + Ab | 776 | 800 | 280 | Gl (+ Fo + En + Ab) |
| mix | 785 | 800 | 717 | Gl (+ Fo + En? + Ab) |
| Fo + En + Ab | 803 | 820 | 187 | Gl (+ Fo + En + Ab) |
| mix | 803 | 820 | 187 | Gl (+ Fo + En? + Ab) |
| Fo + En + Ab + Gl | 833 | 800 | 159 | Gl (+ Fo + En + Ab) |
| mix | 840 | 825 | 168 | Gl (+ Fo + En + Ab) |
| Fo + En + Ab | 850 | 825 | 185 | Gl (+ Fo + En + Ab) |
| mix | 850 | 825 | 185 | Gl (+ Fo + En + Ab) |
| glass | 815 | 1000 | 1920 | Gl (+ Ab + M) |
| mix | 822 | 1000 | 208 | Gl (+ Fo + En? + Ab + M) |
| mix | 835 | 1005 | 93 | Gl (+ Fo + En + Ab) |
| Fo + En + Ab + Gl | 835 | 950 | 313 | Gl (+ Fo + En + Ab) |
| Fo + En + Ab + Gl | 840 | 950 | 315 | Gl (+ Fo + En + Ab) |
| mix | 843 | 1030 | 142 | Gl (+ Fo + En + Ab) |
| mix | 846 | 1000 | 89 | Gl (+ Fo + En + Ab) |
| mix | 821 | 1210 | 64 | Gl (+ Fo + En + Ab) |
| mix | 826 | 1200 | 142 | Gl (+ Fo + En + Ab) |
| mix | 846 | 1200 | 142 | Gl (+ Fo + En + Ab) |
| mix | 846 | 1300 | 25 | Gl (+Fo + En? + Ab) |
| Fo + En + Ab | 859 | 1310 | 66 | Gl (+ Fo + En + Ab) |
| mix | 797 | 1500 | 355 | Gl (+ Fo? + En + Ab + M) |
| mix | 843 | 1490 | 142 | Gl (+ Fo + L) |
| mix | 857 | 1690 | 10 | Gl (+ Fo + En + Ab? + L) |
| glass | 760 | 2000 | 221 | Gl (+ Fo + En + Ab) |

TABLE 7 (Continued)

| Condensed Starting Material | Temp. in °C | $P_{vapor}$ in bars | Duration in hours | Condensed Run Products |
|---|---|---|---|---|
| mix | 794 | 2000 | 20 | (En + Ab + M) |
| mix | 794 | 2000 | 285 | Gl (+ En + Ab + M) |
| mix | 794 | 2000 | 766 | Gl (+ En + Ab + M) |
| Fo + En + Ab | 794 | 2000 | 766 | Gl (+ En + Ab + M) |
| mix | 818 | 2000 | 210 | Gl (+ Fo + En + Ab) |
| mix | 823 | 2000 | 264 | Gl (+ Fo + L) |
| Fo + En + Ab | 843 | 2000 | 94 | (Fo + En + Ab + M) |
| Fo + En + Ab | 857 | 1980 | 18 | (Fo + En + L + M?) |
| mix | 862 | 1990 | 2 | Gl (+ Fo + En + L) |
| mix | 602 | 2500 | 1102 | Gl (+ Ab + M) |
| mix | 652 | 2500 | 870 | Gl (+ Ab + M) |
| mix | 701 | 2520 | 741 | Gl (+ Ab + M) |
| mix | 377 | 4650 | 1129 | (Ab + M) |
| mix | 502 | 4400 | 1104 | Gl? (+ Ab + M) |
| | Curve: Fo + En + Gl + L + V | | | |
| mix | 857 | 1520 | 100 | Gl (+ Fo + En + Ab) |
| mix | 867 | 1490 | 99 | Fo + En + Ab + L |
| Fo + En + Ab | 868 | 1500 | 79 | Fo + En + L |
| mix | 863 | 1690 | 14 | Gl (+ Fo + En + L) |
| Fo + En + Gl + L | 869 | 1700 | 5 | Fo + En + L |
| mix | 862 | 1875 | 6 | Gl (+ Fo + En? + M) |
| Fo + En + L | 862 | 1990 | 2 | Gl (+ Fo + En + L) |
| Fo + En + Gl + L | 866 | 1980 | 2 | Gl (+ Fo + En + L) |
| Fo + En + Gl + L | 873 | 1980 | 2 | Fo + En + L |
| | Field: Fo + En + L + V | | | |
| mix | 879 | 1960 | 5 | Fo + En? + L |
| Fo + En + Ab | 879 | 1960 | 5 | Fo + En + L |
| | Curve: Fo + En + Ab + L + V | | | |
| glass | 986 | 300 | 115 | Fo + En + Ab |
| Fo + En + Ab | 997 | 295 | 162 | Fo + Ab + L |
| glass | 997 | 295 | 162 | Fo + Ab + L |
| Fo + En + Ab | 955 | 510 | 92 | Fo + En + Ab |
| glass | 955 | 510 | 92 | Fo + En + Ab (+ L) |
| Fo + En + Ab | 964 | 510 | 93 | Fo + En + Ab? + L |
| glass | 964 | 510 | 93 | Fo + En + L |
| glass | 915 | 800 | 120 | Fo + En + Ab |
| glass | 891 | 1000 | 115 | Fo + En + Ab |
| Fo + En + Ab | 908 | 1010 | 77 | Fo + En + L |
| glass | 909 | 1000 | 135 | Fo + En + L |
| mix | 857 | 1520 | 100 | Gl (+ Fo + En + Ab) |
| mix | 867 | 1490 | 99 | Fo + En + Ab + L |
| Fo + En + Ab | 868 | 1500 | 79 | Fo + En + L |
| Fo + En + Ab | 843 | 2000 | 94 | (Fo + En + Ab + M) |
| Fo + En + Ab | 857 | 1980 | 18 | (Fo + En + L + M?) |
| | Field: Fo + En + Ab + V | | | |
| mix | 803 | 1 | 330 | Fo + En + Ab |
| mix | 890 | 1 | 2215 | Fo + En + Ab |
| mix | 929 | 1 | 234 | Fo + En + Ab |
| mix | 983 | 1 | 162 | Fo + En + Ab |
| glass | 1074 | 1 | 46 | Fo + En + Ab (+ L) |
| mix | 882 | 260 | 232 | Fo + En + Ab |
| mix | 898 | 270 | 99 | Fo + En + Ab |
| glass | 912 | 300 | 161 | Fo + En + Ab |
| glass | 940 | 293 | 191 | Fo + En + Ab |

TABLE 7 (Continued)

| Condensed Starting Material | Temp. in °C | $P_{vapor}$ in bars | Duration in hours | Condensed Run Products |
|---|---|---|---|---|
| glass | 948 | 293 | 191 | Fo + En? + Ab |
| glass | 960 | 300 | 66 | Fo + En + Ab |
| glass | 975 | 300 | 135 | Fo + En + Ab |
| glass | 925 | 500 | 190 | Fo + En + Ab |
| glass | 931 | 450 | 122 | Fo + En + Ab |
| glass | 939 | 450 | 122 | Fo + En + Ab |
| glass | 902 | 755 | 164 | Fo + En + Ab |
| | Curve: Fo + Ab + L + V | | | |
| Fo + En + Ab | 997 | 295 | 162 | Fo + Ab + L |
| glass | 997 | 295 | 162 | Fo + Ab + L |
| Fo + En + Ab | 1005 | 300 | 120 | Fo + L |
| glass | 1005 | 300 | 120 | Fo + L |
| | Field: Fo + Ab + L + V | | | |
| Fo + En + Ab | 997 | 295 | 162 | Fo + Ab + L |
| glass | 997 | 295 | 162 | Fo + Ab + L |
| | Curve: Fo + En + L + V | | | |
| Fo + En + Ab | 955 | 510 | 92 | Fo + En + Ab (+ L) |
| glass | 955 | 510 | 92 | Fo + En + Ab (+ L) |
| Fo + En + Ab | 964 | 510 | 93 | Fo + En + Ab? + L |
| glass | 964 | 510 | 93 | Fo + En + L |
| | Curve: Fo + En + L + V | | | |
| Fo + En + Ab | 920 | 1010 | 77 | Fo + En + L |
| Fo + En + Ab | 899 | 1400 | 76 | Fo + En? + L |
| Fo + En + Ab | 905 | 1520 | 4 | Fo + L |
| Fo + En + Ab | 888 | 2000 | 4 | Fo + En + L |
| Fo + En + Ab | 896 | 1980 | 4 | Fo + L |
| | Field: Fo + L + V | | | |
| Fo + En + Ab | 1028 | 300 | 120 | Fo + L |
| Fo + En + Ab | 900 | 2000 | 4 | Fo + L |

### *Metastable Sodic Montmorillonite*

Difficulties arose from the formation of a fine-grained hydrous silicate within the glaucophane field at temperatures as high as approximately 850°C at 2000 bars vapor pressure. As indicated in table 9, this phase has the X-ray properties of a member of the montmorillonite group. The basal spacing of 15.3 Å is reduced to 12.3 Å either by heat treatment or by quenching runs at diminished pressure. Basal spacings of approximately 17 Å have been obtained by treatment with ethylene glycol. Complete decomposition of this phase at 900°C and 1 atm total pressure yields enstatite + minor nepheline; weight loss indicates that the material with a basal spacing of 12.3 Å contains 6 ± 2 weight percent $H_2O$. From the relative proportions of breakdown products deduced by X-ray and optical examination, the montmorillonite is estimated to have the approximate formula: $Na_{1/2}Mg_3Al_{1/2}Si_{3\text{-}1/2}O_{10}(OH)_2 \cdot nH_2O$.

Stability relations for minerals of the montmorillonite group presented by Ames and Sand (1958) indicate that soda-bearing trioctahedral varieties are stable at elevated temperatures. At 1000 atm vapor pressure, montmorillonite

TABLE 8

Results of investigation of the composition $Na_2O \cdot 3MgO \cdot Al_2O_3 \cdot 10SiO_2$ with excess water

| Condensed Starting Material | Temp. in °C | $P_{vapor}$ in bars | Duration in hours | Condensed Run Products |
|---|---|---|---|---|
| | | Curve: En + Ab + Q + Gl + V | | |
| En + Ab + Q | 847 | 150 | 403 | En + Ab + Q |
| Tc + Ab | 843 | 245 | 187 | Q (+ En + Ab) |
| mix | 843 | 245 | 187 | Gl (+ En + Ab + L) |
| En + Ab + Q + Gl | 852 | 250 | 991 | En + Ab + Q + Gl |
| Tc + Ab | 842 | 515 | 134 | Q + Gl? (+ En + Ab + M) |
| mix | 842 | 515 | 134 | Gl (+ En + Ab + L) |
| Tc + Ab | 855 | 490 | 234 | En + Ab + Q |
| mix | 855 | 490 | 234 | En + Ab + Q + Gl |
| Tc + Ab | 866 | 490 | 234 | En + Ab + Q |
| | | Field: Q + Gl + V | | |
| mix | 827 | 250 | 160 | Q? + Gl (+ En + Ab + L) |
| mix | 792 | 505 | 280 | Q? + Gl (+ En + Ab) |
| Tc + Ab | 800 | 500 | 241 | Q + Gl (+ En + Ab) |
| Tc + Ab | 814 | 505 | 280 | Q + Gl (+ En + Ab) |
| mix | 814 | 505 | 280 | Q + Gl (+ En + Ab) |
| Tc + Ab | 807 | 1010 | 278 | Q + Gl? (+ En + Ab) |
| Tc + Ab | 815 | 1000 | 1920 | Q + Gl (+ En + Ab + M) |
| mix | 770 | 1505 | 170 | Q + Gl (+ En + Ab + M) |
| mix | 702 | 2020 | 240 | Q + Gl (+ En + Ab) |
| | | Curve: En + Q + Gl + L + V | | |
| Tc + Ab | 817 | 1000 | 622 | Q + Gl (+ En + Ab) |
| Tc + Ab | 823 | 1000 | 311 | En + Q + Gl + L (+ Ab) |
| Tc + Ab | 827 | 1005 | 356 | En + Gl + L (+ Ab) |
| mix | 827 | 1005 | 356 | En + Gl + L |
| En + Ab + Q | 782 | 1500 | 494 | En + Q + L (+ Ab + M) |
| mix | 782 | 1500 | 494 | Gl + L (+ Ab + M) |
| Tc + Ab | 789 | 1510 | 474 | En + Q + Gl + L (+ Ab + Tc + M) |
| En + Ab + Q | 789 | 1510 | 474 | En + Q + Gl? + L? (+ Ab) |
| Tc + Ab | 792 | 1500 | 480 | En + Gl + L (+ Ab + M) |
| En + Ab + Q | 792 | 1500 | 480 | En + Gl + L (+ Ab + M) |
| En + Ab + Q | 745 | 2000 | 332 | Q + Gl (+ En + Ab + M) |
| mix | 745 | 2000 | 332 | Q? + Gl (+ En + Ab + L) |
| En + Ab + Q | 756 | 1995 | 440 | En + Q + Gl + L (+ Ab + M) |
| mix | 756 | 1995 | 440 | En + Gl + L (+ Ab) |
| En + Ab + Q | 763 | 2000 | 438 | En + Gl + L (+ Ab) |
| mix | 763 | 2000 | 438 | En + Gl + L (+ Ab) |
| | | Field: En + Gl + L | | |
| Tc + Ab | 839 | 1000 | 87 | En + L (+ Ab) |
| mix | 839 | 1000 | 87 | En + Gl + L |
| mix | 841 | 1175 | 240 | En + Gl + L |
| Tc + Ab | 836 | 1730 | 38 | En + Gl + L (+ Tc) |
| mix | 836 | 1730 | 38 | En + Gl + L |
| En + Ab + Q | 770 | 2000 | 428 | En + Gl + L (+ Ab) |
| En + Ab + Q | 780 | 1990 | 264 | En + Gl? + L (+ Ab + M) |
| mix | 780 | 1990 | 264 | En + Gl + L (+ Ab + M) |
| En + Ab + Q | 795 | 2000 | 325 | En + Gl + L (+ Ab + M) |
| Tc + Ab | 811 | 2020 | 239 | En + Gl? + L (+ Ab + M) |
| mix | 811 | 2020 | 239 | En + Gl + L (+ Ab) |
| Tc + Ab | 820 | 2000 | 151 | En + L (+ Ab + M) |

TABLE 8 (Continued)

| Condensed Starting Material | Temp. in °C | $P_{vapor}$ in bars | Duration in hours | Condensed Run Products |
|---|---|---|---|---|
| mix | 820 | 2000 | 151 | En + Gl + L (+ Ab) |
| Tc + Ab | 832 | 1990 | 48 | En + L (+ M) |
| mix | 832 | 1990 | 48 | En + Gl + L |
| mix | 843 | 2000 | 33 | En + Gl + L |
| mix | 851 | 1990 | 3 | En + Gl + L |
| | | Curve: En + Gl + L + V | | |
| Tc + Ab | 860 | 1500 | 21 | En + Gl + L (+ Tc) |
| mix | 860 | 1500 | 21 | En + Gl + L |
| En + Tc + Gl + L | 868 | 1520 | 49 | En + L |
| En + Gl + L | 868 | 1520 | 49 | En + Gl? + L |
| En + Ab + Gl + L | 861 | 1990 | 2 | En + Gl + L |
| En + Gl + L | 863 | 2000 | 6 | En + Gl + L |
| mix | 863 | 2000 | 6 | En + Gl + L |
| En + Gl + L | 868 | 1995 | 4 | En + L |
| mix | 868 | 1995 | 4 | En + L (+Gl?) |
| | | Field: En + L + V | | |
| Tc + Ab | 967 | 505 | 119 | En + L (+ Fo?) |
| En + Ab + Q | 950 | 810 | 23 | En + L (+ Fo?) |
| Tc + Ab | 925 | 995 | 93 | En + L |
| En + Ab + Q | 910 | 2000 | 1 | En + L |
| | | Field: Fo + En + L + V | | |
| Tc + Ab | 1005 | 500 | 22 | Fo + En + L |
| | | Curve: En + Ab + L + V | | |
| Tc + Ab | 945 | 500 | 187 | En + Ab + L |
| Tc + Ab | 882 | 990 | 112 | En + Ab? + L |
| Tc + Ab | 897 | 995 | 116 | En + L (+ M) |
| En + Ab + Q | 897 | 995 | 116 | En + L (+M) |
| Tc + Ab | 869 | 1200 | 162 | En + Ab + L (+ M) |
| | | Field: En + Ab + L + V | | |
| Tc + Ab | 924 | 515 | 97 | En + Ab + L |
| | | Curve: En + Ab + Gl + L + V | | |
| mix | 851 | 995 | 163 | En + Ab? + Gl + L |
| Tc + Ab | 860 | 1015 | 103 | En + Ab + L |
| mix | 860 | 1015 | 103 | En + Gl + L |
| Tc + Ab | 870 | 1000 | 87 | En + Ab + L |
| mix | 870 | 1000 | 87 | En + Ab? + L |
| Tc + Ab | 860 | 1200 | 162 | En + Ab + Gl? + L (+ M) |
| Tc + Ab | 869 | 1200 | 162 | En + Ab + L (+ M) |
| | | Field: En + Ab + Q + V | | |
| Tc + Ab | 913 | 1 | 24 | En + Ab + Q |
| Tc + Ab | 899 | 250 | 145 | En + Ab + Q |
| Tc + Ab | 875 | 400 | 911 | En + Ab + Q |
| | | Field: En + Ab + Tr + V | | |
| Tc + Ab | 925 | 245 | 209 | En + Ab + Tr? (+ Q) |
| | | Curve: En + Ab + Tr + L + V | | |
| Tc + Ab | 944 | 250 | 131 | En + Ab + Tr (+ Q) |
| Tc + Ab | 952 | 250 | 70 | En + Ab + L (+ Fo?) |

TABLE 8 (Continued)

| Condensed Starting Material | Temp. in °C | $P_{vapor}$ in bars | Duration in hours | Condensed Run Products |
|---|---|---|---|---|
| | Curve: En + Ab + Q + L + V | | | |
| Tc + Ab | 882 | 515 | 134 | En + Ab + Q + L |
| mix | 882 | 515 | 134 | En + Ab + L |
| Tc + Ab | 900 | 515 | 177 | En + Ab + L |
| | Results of Investigation of the Composition $Na_2O \cdot 3MgO \cdot Al_2O_3 \cdot 9SiO_2$ with Excess Water | | | |
| En + Ab | 850 | 800 | 307 | En + Gl + L (+ Ab + M) |
| En + Ab | 856 | 795 | 306 | En + Gl + L? (+ Ab + M) |
| En + Ab | 866 | 795 | 306 | En + Ab |

TABLE 9

X-ray powder data for metastable phase M compared with synthetic and natural montmorillonite

| Synthetic Montmorillonite, (Saponite), Ames and Sand (1958) | | Synthetic Montmorillonite, present study | | | | Natural Montmorillonite, Nagelschmidt (1938) | |
|---|---|---|---|---|---|---|---|
| | | collapsed spacing | | normal spacing | | | |
| Intensity | d in Å | Intensity | d in Å | Intensity | d in Å | Intensity | d in Å |
| 10 | 12.3 | >10 | 12.3 | >10 | 15.3 | vs | 15.3 |
| 2 | 6.15 | 1 | 6.1 | 1 | 7.6 | — | — |
| 4 | 4.58 | 2 | 4.58 | 1 | 5.01 | s | 5.15 |
| 5 | 3.10 | 7 | 3.04 | 1 | 4.60 | vs | 4.50 |
| 4 | 2.63 | 2 | 2.64 | 9 | 3.00 | vs | 3.07 |
| 3 | 2.53 | 4 | 2.50 | 1 | 2.61 | vs | 2.61 |
| 1 | 2.34 | — | — | 1 | 2.47 | | 2.55 |
| 1 | 2.295 | 2 | 2.30 | 1 | 2.41 | | 2.41 |
| 1 | 2.067 | 1 | 2.08 | | | | |

Intensities visually estimated.
s = strong.
vs = very strong.

with the formula $Na_{0.33}Mg_{3.00}Al_{0.33}Si_{3.67}O_{10}(OH)_2$ (i.e., saponite) decomposes above 740°C and below 780°C (Ames and Sand, 1958, table 1).

Sodic montmorillonite encountered in the present study is considered metastable because, on long runs, glaucophane slowly grows at its expense (fig. 1).

*Location of Curves*

Figures 3 and 4 are $P_{vapor}$-T plots of the data given in tables 7 and 8 respectively. In figure 4, location of the $\beta$ quartz-tridymite transition was taken from Tuttle and England (1955). $P_{vapor}$-T locations of curves are presented in tables 10 and 11. Each curve has been located at temperatures slightly in excess of those for which the low-temperature assemblage was obtained. This method is based on the observation that although high-temperature assemblages may persist indefinitely at low temperatures, the converse phenomenon (crystal-

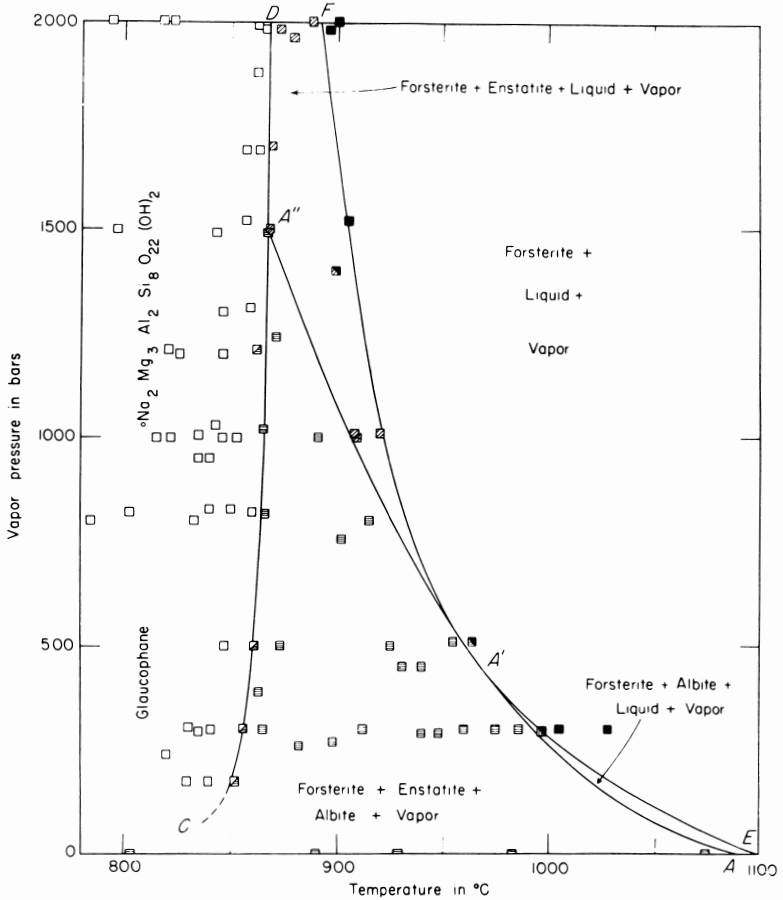


Fig. 3. $P_{vapor}$-T diagram for the composition $Na_2O \cdot 3MgO \cdot Al_2O_3 \cdot 8SiO_2$ + excess water. Divided run symbols indicate presence of the low-temperature assemblage in trace amounts. Curve locations at 1 atm (points A and E) were determined by Schairer and Yoder (1960, and personal communication).

lization of a mineral at temperatures in excess of its stability field) is rare, especially in the $P_{vapor}$-T range investigated.

Oxide mixtures, crystal assemblages, and in some cases glass were employed for the determination of each curve. It was found that oxide mixtures and glass for both investigated bulk compositions yielded melt at temperatures as much as 25° to 50°C lower than obtained using the assemblages forsterite + enstatite + albite, enstatite + albite + quartz, and talc + albite (all with or without glaucophane) previously crystallized from either glass or oxide mixtures. (See table 7, runs at 853°C and 1000 bars $P_{vapor}$, 843°C and 1490 bars $P_{vapor}$, 955°C and 510 bars $P_{vapor}$; table 8, 792°C and 505 bars $P_{vapor}$.) Apparently metastable melt resulted from incomplete reaction.

Curves representing the high-temperature stability limit of glaucophane are believed accurate to within ± 5°C, as shown by reversals of the reaction

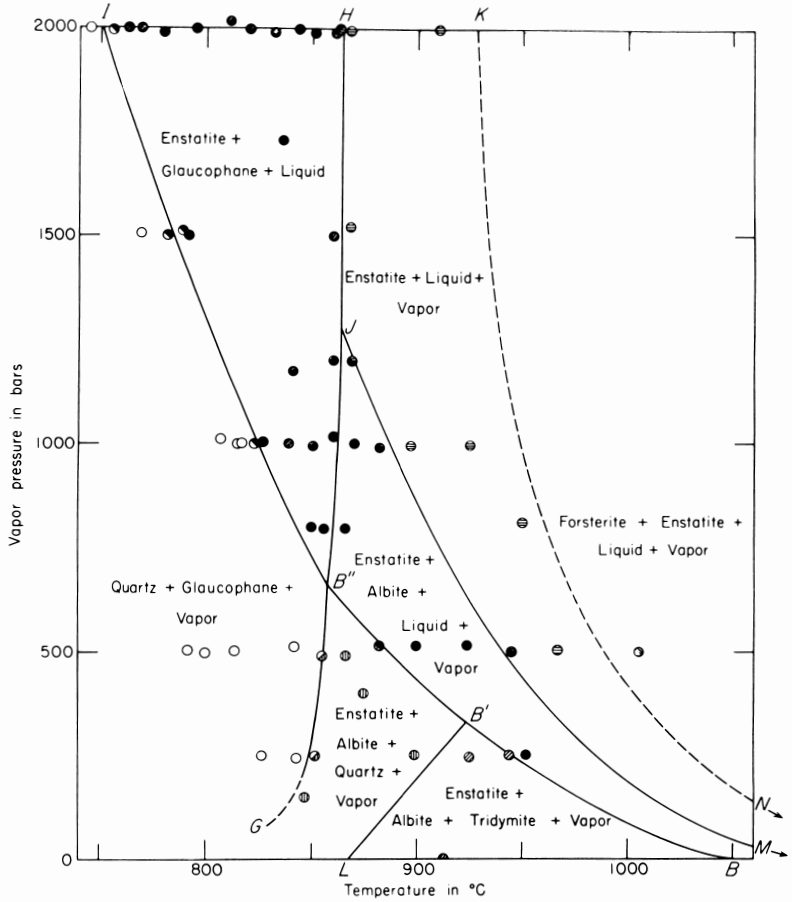


Fig. 4. $P_{vapor}$-T diagram for the composition $Na_2O \cdot 3MgO \cdot Al_2O_3 \cdot 10SiO_2$ + excess water. Divided run symbols indicate presence of the low-temperature assemblage in trace amounts. Curve locations at 1 atm (points B, M, and N) were determined by Schairer and Yoder (1960, and personal communication).

at 820 and 2000 bars vapor pressure for the bulk composition $Na_2O \cdot 3MgO \cdot Al_2O_3 \cdot 8SiO_2$ + excess water, and at 1500 bars vapor pressure for the bulk composition $Na_2O \cdot 3MgO \cdot Al_2O_3 \cdot 10SiO_2$ + excess water. Because the investigation was concerned primarily with amphibole stability, glaucophane field boundaries were determined with greater precision than were those involving equilibria exclusive of glaucophane. These latter curves are considered accurate to $\pm$ 10°C. For the bulk composition glaucophane + vapor, the melting curve of albite between 450 and 1500 bars vapor pressure is known with greater accuracy than is apparent from figure 3. The metastable extension of this curve into the glaucophane field was bracketed between 843° and 857°C at 2000 bars $P_{vapor}$, using the crystal assemblage forsterite + enstatite + albite (see table 7). Glaucophane grows very slowly from this assemblage, and, as it was not detected on these two runs, they are omitted from the phase diagram.

TABLE 10

$P_{vapor}$-T locations of curves presented in figure 3
(bulk composition $Na_2O \cdot 3MgO \cdot Al_2O_3 \cdot 8SiO_2 + H_2O$)

| Curve | $P_{vapor}$ (bars) | Temp. (°C) |
|---|---|---|
| Fo + En + Ab + Gl + V | 175 | 850 ± 5 |
| | 300 | 855 ± 5 |
| | 500 | 859 ± 5 |
| | 820 | 863 ± 5 |
| | 1000 | 864 ± 5 |
| | 1300 | 866 ± 5 |
| | 1500 | 867 ± 5 |
| Fo + En + Ab + L + V | 1* | 1093 ± 5 |
| | 300 | 993 ± 10 |
| | (450) | (968 ± 10) |
| | 500 | 961 ± 10 |
| | 1000 | 906 ± 10 |
| | 1500 | 867 ± 5 |
| Fo + En + Gl + L + V | 1500 | 867 ± 5 |
| | 1700 | 868 ± 5 |
| | 2000 | 868 ± 5 |
| Fo + Ab + L + V | 1* | 1103 ± 5 |
| | 300 | 996 ± 10 |
| | (450) | (968 ± 10) |
| Fo + En + L + V | (450) | (968 ± 10) |
| | 500 | 961 ± 10 |
| | 1500 | 905 ± 10 |
| | 2000 | 892 ± 10 |

* Phase relations at atmospheric pressure determined by Schairer and Yoder (1960, and personal communication).
Parentheses enclose interpolated P-T values.

Stability of glaucophane in this $P_{vapor}$-T region is indicated by numerous runs in which it was obtained, and especially by the experiment at 862°C and 1990 bars $P_{vapor}$, in which glaucophane grew at the expense of the high-temperature equivalent assemblage. The melting curve of albite for the bulk composition quartz + glaucophane + vapor is known with greater accuracy than is apparent from figure 4. The metastable extension of this curve into the field enstatite + glaucophane + liquid was bracketed between 820° and 832°C at 2000 bars vapor pressure (see table 8).

### *Discussion of Phase Diagrams*

To a good approximation, all phases obtained for the investigated bulk compositions fall within the quaternary system $2MgO \cdot SiO_2$–$Na_2O \cdot Al_2O_3 \cdot 6SiO_2$–$SiO_2$–$H_2O$. Any departure of the compositions of liquid and vapor from this system is so small as to produce no measurable change in properties or relative proportions of the crystals. The system $2MgO \cdot SiO_2$–$Na_2O \cdot Al_2O_3 \cdot 6SiO_2$–$SiO_2$–$H_2O$ is shown diagrammatically in figure 5. Phase relations discussed below may be more clearly visualized by reference to this figure.

The shapes of glaucophane $P_{vapor}$-T fields are similar to those of other hydrous silicates, but the high-temperature stability limit of this mineral has a

TABLE 11

$P_{vapor}$-T locations of curves presented in figure 4
(bulk composition $Na_2O \cdot 3MgO \cdot Al_2O_3 \cdot 10SiO_2 + H_2O$)

| Curve | $P_{vapor}$ (bars) | Temp. (°C) |
|---|---|---|
| En + Ab + Q + Gl + V | 250 | 849 ± 5 |
| | 500 | 855 ± 5 |
| | (660) | (857 ± 5) |
| En + Ab + Tr + L + V | 1* | 1050 ± 10 |
| | 250 | 946 ± 10 |
| | (330) | (924 ± 10) |
| En + Ab + Q + L + V | (330) | (924 ± 10) |
| | 500 | 887 ± 10 |
| | (660) | (857 ± 5) |
| En + Q + Gl + L + V | (660) | (857 ± 5) |
| | 1000 | 825 ± 5 |
| | 1500 | 785 ± 5 |
| | 2000 | 751 ± 5 |
| En + Ab + Gl + L + V | (660) | (857 ± 5) |
| | 800 | 859 ± 5 |
| | 1000 | 861 ± 5 |
| | 1200 | 863 ± 5 |
| | (1280) | (863 ± 5) |
| En + Ab + L + V | 1* | 1103 ± 5 |
| | 500 | 941 ± 10 |
| | 1000 | 887 ± 10 |
| | 1200 | 870 ± 10 |
| | (1280) | (864 ± 5) |
| En + Gl + L + V | (1280) | (864 ± 5) |
| | 1500 | 864 ± 5 |
| | 2000 | 865 ± 5 |
| Fo + En + L + V | 1* | 1152 ± 5 |
| | 500 | 990 ± 10 |

* Phase relations at atmospheric pressure determined by Schairer and Yoder (1960 and personal communication).
Parentheses enclose interpolated P-T values.

very steep dP/dT slope. An additional complexity appears in the phase diagram for the composition $Na_2O \cdot 3MgO \cdot Al_2O_3 \cdot 10SiO_2$ + excess water where glaucophane coexists with melt in a divariant region.

Fig. 5. Diagrammatic representation of liquidus surfaces in the system $2MgO \cdot SiO_2$–$Na_2O \cdot Al_2O_3 \cdot 6SiO_2$–$SiO_2$–$H_2O$ at pressures of (a) 1 atm total pressure, (b) 450 bars $P_{vapor}$, and (c) 2000 bars $P_{vapor}$. The $H_2O$ apex is towards the reader, and liquidus surfaces are projected onto the ternary face $2MgO \cdot SiO_2$–$Na_2O \cdot Al_2O_3 \cdot 6SiO_2$–$SiO_2$. Preliminary results obtained at 1 atm total pressure by Schairer and Yoder (1960, and personal communication) are the basis for 5a. Details of the protoenstatite-orthoenstatite inversion and location of the two-liquid region at high silica values have been omitted for simplicity. Liquidus relations at elevated vapor pressures are inferred from crystallization sequences and treatment of invariant points for the compositions $Na_2O \cdot 3MgO \cdot Al_2O_3 \cdot 8SiO_2 + H_2O$ (indicated by +) and $Na_2O \cdot 3MgO \cdot Al_2O_3 \cdot 10SiO_2 + H_2O$ (indicated by x). Glaucophane becomes stable in the presence of melt at 858°C and 660 bars $P_{vapor}$ (fig. 4, point B″); with increasing vapor pressure, the primary crystallization field of amphibole expands and reaches the composition of the quaternary reaction point (fig. 3, point A″) at 867°C and 1500 bars.

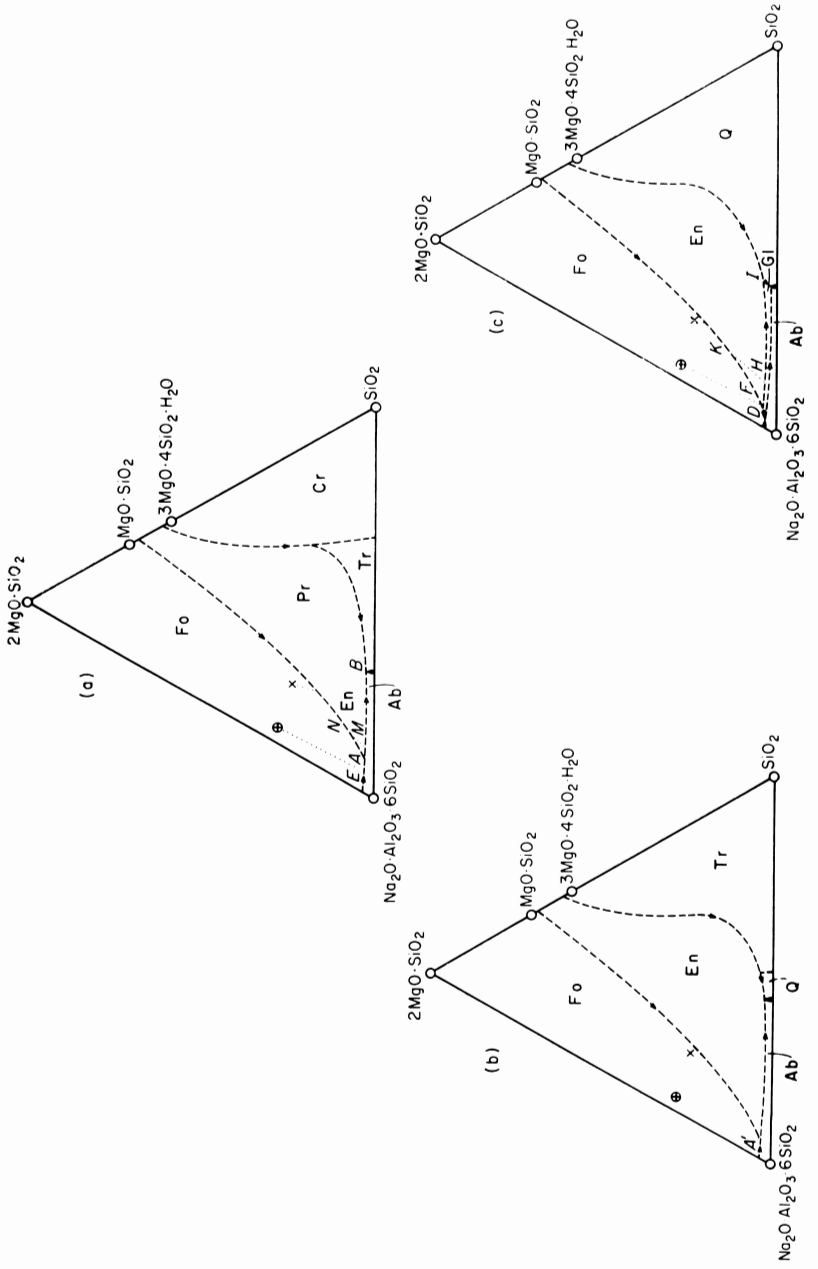
2MgO·SiO2
MgO·SiO2
3MgO·4SiO2·H2O
SiO2
Na2O·Al2O3·6SiO2
Ab
Fo
Pr
Cr
Tr
En
Q
Gl
(a)
(b)
(c)
wt per cent

**Fig. 5**

*Glaucophane + vapor.*—At low vapor pressures the high-temperature assemblage adjoining that of glaucophane consists of forsterite, enstatite, albite, and vapor. Schairer and Yoder (1960, and personal communication) determined the melting behavior at 1 atm for the composition $Na_2O \cdot 3MgO \cdot Al_2O_3 \cdot 8SiO_2$ (points A and E in figs. 3 and 5a). They found that below 1093°±5°C the stable assemblage for this bulk composition consists of forsterite, albite, and $MgO \cdot SiO_2$, between 1093° ± 5°C and 1103° ± 5°C of forsterite, albite, and liquid, and above 1103° ± 5°C of forsterite and liquid. These authors place the ternary reaction point (A in figs. 3 and 5a) at 1098° ± 5°C (personal communication) and the forsterite-albite binary eutectic at 1100° ± 5°C, so the temperatures of A and E in figure 3 are probably between 1093° and 1098°C and between 1098° and 1100° respectively. For this bulk composition, the melting curves of albite (EA′) and enstatite (AA′) become tangent (point A′) at 968°C and 450 bars $P_{vapor}$; with pressures in excess of this amount, albite melts at a lower temperature than enstatite. At 1500 bars $P_{vapor}$ and 867°C (point A″) the albite melting curve (A′A″) intersects the high-temperature stability limit of glaucophane (CA″D); with greater vapor pressure forsterite, enstatite, liquid, and vapor are the high-temperature assemblage adjacent to the glaucophane field. A break in slope of the glaucophane field boundary must occur at the 1500 bar point since the two different reactions involving glaucophane should have different $\Delta S/\Delta V$ values; however, as figure 3 shows, within experimental limits of error, this discontinuity is undetectable.

The low-temperature melting curves (that of enstatite below 450 bars $P_{vapor}$, and that of albite at vapor pressures greater than 450 bars) represent the $P_{vapor}$-T migration of the quaternary reaction liquid (melt in equilibrium with forsterite, enstatite, albite, and vapor) in the system $2MgO \cdot SiO_2$–$Na_2O \cdot Al_2O_3 \cdot 6SiO_2$–$SiO_2$–$H_2O$. This migration (curve AA′A″) must proceed along a smooth P-T curve, independent of bulk composition. Although with increasing vapor pressure the binary eutectic between albite and silica is displaced towards the component $SiO_2$, compared to the "dry" data (Tuttle and Bowen, 1958, p. 52), the composition of the quaternary reaction liquid must move towards the component $Na_2O \cdot Al_2O_3 \cdot 6SiO_2$ to produce the observed intersection of the melting curves of albite and enstatite (fig. 5). The simultaneous appearance of enstatite and albite in equilibrium with forsterite and liquid occurs at the vapor pressure where the composition of forsterite, the bulk composition, and quaternary reaction liquid (A′) lie on a straight line in the ternary projection (fig. 5b). It is suggested that the peritectic between forsterite and enstatite retreats towards the $2MgO \cdot SiO_2$ apex at elevated vapor pressure, causing expansion of the primary crystallization field of enstatite. An alternative explanation is that the forsterite-enstatite field boundary does not change appreciably, but the eutectic between forsterite and albite migrates towards the $Na_2O \cdot Al_2O_3 \cdot 6SiO_2$ apex.

From figure 5 it is apparent that the contemporaneous beginning of crystallization of enstatite and albite in the presence of forsterite will occur at a specific vapor pressure and temperature for a particular bulk composition. For a composition richer in silica than $Na_2O \cdot 3MgO \cdot Al_2O_3 \cdot 8SiO_2$, this point lies on the $P_{vapor}$-T curve for the quaternary reaction liquid at a vapor pressure

less than 450 bars. The described intersection of P-T curves is a point on a univariant P-T-x curve (not shown in figure 3) along which the five phases forsterite, enstatite, albite, liquid, and vapor coexist. The single degree of freedom (five phases present in a four-component system) indicates that for a range of bulk compositions, and therefore a range of vapor pressures, the crystallization path proceeds through the forsterite field directly to the location of the quaternary reaction liquid, where enstatite and albite simultaneously become stable.

*Quartz + glaucophane + vapor.*—At low vapor pressures the high-temperature assemblage adjoining that of quartz + glaucophane + vapor consists of enstatite, albite, quartz, and vapor. Schairer and Yoder (1960, and personal communication) determined liquidus-solidus relations for the composition $Na_2O \cdot 3MgO \cdot Al_2O_3 \cdot 10SiO_2$ at atmospheric pressure (points B, M, and N in figs. 4 and 5a) and found that below 1050° ± 10°C the stable assemblage consists of enstatite, albite, and tridymite; between 1050° ± 10°C and 1103° ± 5°C, of enstatite, albite, and liquid; between 1103° ± 5°C and 1152° ± 5°C, of $MgO \cdot SiO_2$ and liquid; and above 1152° ± 5°C, of forsterite + $MgO \cdot SiO_2$ + liquid. The 1 atm melting relations quoted are the actual temperature values obtained by Schairer and Yoder for the bulk compositions $Na_2O \cdot 3MgO \cdot Al_2O_3 \cdot 8SiO_2$ and $Na_2O \cdot 3MgO \cdot Al_2O_3 \cdot 10SiO_2$. Inspection of figure 5a indicates that the liquidus temperature of point E must exceed that of A which in turn has a value higher than that of M.

As shown in figure 5, with decreasing temperature crystallization commences with forsterite, joined at slightly lower temperatures by $MgO \cdot SiO_2$. The quaternary reaction point (in projection) lies to the left of the extension of the join connecting $MgO \cdot SiO_2$ and $Na_2O \cdot 3MgO \cdot Al_2O_3 \cdot 10SiO_2$. Thus, as heat is subtracted from the system, forsterite reacts with melt to form additional enstatite and is completely used up as the liquid reaches the composition N (at 1 atm total pressure), or K (at 2000 bars $P_{vapor}$). On further cooling, the liquid leaves the forsterite field boundary and moves through the primary field of crystallization of enstatite directly away from the composition $MgO \cdot SiO_2$ to the junction with the albite field boundary (M in fig. 5a) or the primary field of crystallization of glaucophane (H in fig. 5c). The migration of the liquid through the enstatite field is indicated in figure 4 by the assemblage enstatite + liquid + vapor.

The eutectic in the system $2MgO \cdot SiO_2$–$Na_2O \cdot Al_2O_3 \cdot 6SiO_2$–$SiO_2$–$(H_2O)$ is at point B in figure 5a; liquid of this composition is in equilibrium with enstatite, albite, a silica mineral (and vapor). The $P_{vapor}$-T migration of this minimum is shown in figure 4 as curve BB′B″. At 924°C and 330 bars vapor pressure (point B′) this curve intersects the curve for the $\beta$ quartz-tridymite transition. Because of differences in volumes and entropies of these two latter phases, the minimum melting curve should exhibit a discontinuity in slope, but as indicated in figure 4 the inflection is slight.

The minimum melting curve intersects the high-temperature stability limit of glaucophane at 857°C and 660 bars $P_{vapor}$ (point B″). Treatment of this point (see section on invariant points and fig. 7) indicates that the high-temperature amphibole stability limit below 660 bars $P_{vapor}$ (curve GB″) has

a steeper dP/dT slope than the glaucophane boundary at vapor pressures in excess of this amount (curve B″J). Qualitatively this inflection may be visualized by consideration of reactions involved. Curve GB″ defines the univariant curve for the reaction (1) Q + Gl → En + Ab + V, and curve B″J, the reaction (2) Gl + L → En + Ab + V. Only phases taking part in the reactions are specified. Products in both reactions are the same phases. The reactants in (2) are more hydrous than those of (1). Hence because of the evolution of vapor, $\Delta V_{Gl + L \rightarrow En + Ab + V}$ is greater than $\Delta V_{Q + Gl \rightarrow En + Ab + V}$. Reaction (2) proceeds with a smaller ΔS than (1) because entropy of the liquid is greater than that of quartz. Therefore, the curve defining the high-temperature stability limit of glaucophane above 660 bars $P_{vapor}$ must have a smaller value of $\Delta S/\Delta V$, and hence a more gentle dP/dT slope than that of the curve below 660 bars.

At temperatures in excess of curve B″J, albite + enstatite are stable in the presence of vapor. However, below this curve all the albite and part of the enstatite react with vapor to produce glaucophane and small amounts of melt. This unusual behavior is verified by experiments performed on the composition $Na_2O \cdot 3MgO \cdot Al_2O_3 \cdot 9SiO_2$ + excess $H_2O$ (enstatite + albite + vapor). Run data are presented at the end of table 8. At still lower temperatures (below curve B″I) quartz, additional glaucophane, and vapor are produced at the expense of all the remaining enstatite and liquid.

Intersection of the albite melting curve with the high-temperature glaucophane stability limit at 863°C, 1280 bars $P_{vapor}$ (point J in fig. 4) gives rise to another inflection in the amphibole boundary due to differences in ΔV and ΔS for reactions involving glaucophane. At vapor pressures in excess of this intersection, the high-temperature stability limit of glaucophane (JH) has a nearly vertical dP/dT slope, as indicated in figure 4.

## THERMODYNAMIC CONSIDERATIONS

### *Application of Phase Theory to Glaucophane $P_{vapor}$-T Curves*

*Glaucophane + vapor.*—Experimental investigation of the composition $Na_2O \cdot 3MgO \cdot Al_2O_3 \cdot 8SiO_2$ with excess water located an invariant point in the system $2MgO \cdot SiO_2$–$Na_2O \cdot Al_2O_3 \cdot 6SiO_2$–$SiO_2$–$H_2O$ at 867°C and 1500 bars, where forsterite, enstatite, albite, glaucophane, liquid, and vapor coexist. The anhydrous composition of the liquid was determined utilizing the crystallization sequence obtained in this study together with data on the ternary system $2MgO \cdot SiO_2$–$Na_2O \cdot Al_2O_3 \cdot 6SiO_2$–$SiO_2$ (Schairer and Yoder, 1960, and personal communication). Water content of the liquid, 5 ± 2 weight percent, was determined by dehydrating glass quenched from the conditions $P_{vapor}$ = 1500 bars, T = 868°C. The vapor was assumed to be nearly pure $H_2O$, inasmuch as glass droplets (which would result from condensation of a silica-rich vapor) were never observed.

Six univariant curves, along each of which five phases are stable, terminate at this invariant point. The reactions defining the curves are:

Glaucophane = forsterite + enstatite + albite + vapor (L)
Enstatite + albite + vapor = forsterite + liquid (Gl)
Forsterite + enstatite + liquid + vapor = glaucophane (Ab)

Forsterite + liquid + vapor = albite + glaucophane (En)
Forsterite + liquid = enstatite + albite + glaucophane (V)
Glaucophane + liquid = enstatite + albite + vapor (Fo)

These reactions were obtained by constructing joins and three-phase triangles within the tetrahedron $2MgO \cdot SiO_2$–$Na_2O \cdot Al_2O_3 \cdot 6SiO_2$–$SiO_2$–$H_2O$, and checked using algebraic and graphical methods described by Niggli (1954, p. 403-411). Each curve is designated by enclosing in parentheses the symbol for the phase which does not take part in the reaction. Only three of these curves

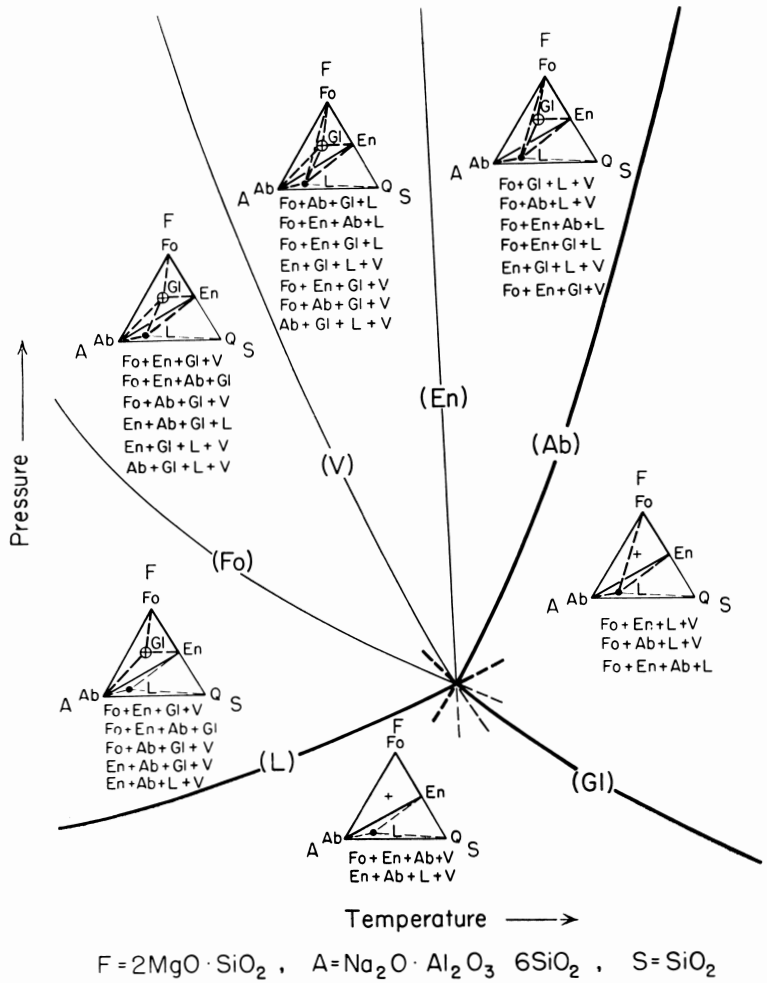


$F = 2MgO \cdot SiO_2$ , $A = Na_2O \cdot Al_2O_3 \cdot 6SiO_2$ , $S = SiO_2$

Fig. 6. Schematic arrangement of all possible curves that terminate at the invariant $Al_2O_3 \cdot 6SiO_2$-point at 867°C, 1500 bars vapor pressure, in the system $2MgO \cdot SiO_2$–$Na_2O \cdot SiO_2$–$H_2O$. Diagrammatic tetrahedra (in mole percent) indicate phase compatibilities between curves. Heavy joins and listed assemblages are appropriate for the subsystem undersaturated with respect to silica. Solid joins lie on the plane $2MgO \cdot SiO_2$–$Na_2O \cdot Al_2O_3 \cdot 6SiO_2$–$SiO_2$; dashed joins lie within the quaternary system $2MgO \cdot SiO_2$–$Na_2O \cdot Al_2O_3 \cdot 6SiO_2$–$SiO_2$–$H_2O$. Joins with vapor have been omitted.

are shown in figure 3, because changes of bulk composition are necessary to obtain (Fo) and (En) experimentally, and (V) can be realized only by exclusion of the vapor phase (prohibited by the experimental technique). The coincidence theorem of Morey and Williamson (1918) indicates that curve (En) lies between (V) and (Ab), curve (Fo) lies between (L) and (V), and that one or more curves lie between (Fo) and (Gl). In figure 6 the arrangement of all possible curves is presented schematically.

Tetrahedra (also shown diagrammatically in mole percent for clarity) for the system $2MgO \cdot SiO_2$–$Na_2O \cdot Al_2O_3 \cdot 6SiO_2$–$SiO_2$–$H_2O$ with water-bearing phases projected onto the plane of the paper ($2MgO \cdot SiO_2$–$Na_2O \cdot Al_2O_3 \cdot 6SiO_2$–$SiO_2$) indicate phase relations between the curves. All phases considered (except liquid) lie within the subsystem $2MgO \cdot SiO_2$–$MgO \cdot SiO_2$–$Na_2O \cdot Al_2O_3 \cdot 6SiO_2$–$H_2O$. Silica-saturated assemblages are indicated by lighter lines. Solid joins lie on the ternary face $2MgO \cdot SiO_2$–$Na_2O \cdot Al_2O_3 \cdot 6SiO_2$–$SiO_2$; broken tie lines lie within the tetrahedron. Joins with the $H_2O$ apex are not shown. With or without vapor, glaucophane is stable in all areas at lower temperature than curve (Ab) and at higher pressure than curve (L). In addition to the projected tetrahedra, figure 6 lists all possible phase assemblages within the "subsystem" undersaturated with respect to silica for each P-T field.

*Quartz + glaucophane + vapor.*—Experimental investigation of the composition $Na_2O \cdot 3MgO \cdot Al_2O_3 \cdot 10SiO_2$ with excess water located two more invariant points in the system $2MgO \cdot SiO_2$–$Na_2O \cdot Al_2O_3 \cdot 6SiO_2$–$SiO_2$–$H_2O$, one at 857°C and 660 bars, where enstatite, albite, quartz, glaucophane, liquid, and vapor are stable, the other at 924°C and 330 bars, where enstatite, albite, quartz, tridymite, liquid, and vapor coexist. Dehydration of glass quenched from the conditions $P_{vapor} = 1000$ bars, T = 870°C, yields a value of approximately $6 \pm 3$ weight percent $H_2O$. Treatment of these invariant points was carried out as described above.

The six curves which intersect at 857°C and 660 bars are defined by the univariant equilibria:

| | |
|---|---|
| Quartz + glaucophane = enstatite + albite + vapor | (L) |
| Enstatite + albite + quartz + vapor = liquid | (Gl) |
| Enstatite + albite + vapor = glaucophane + liquid | (Q) |
| Enstatite + albite + liquid = quartz + glaucophane | (V) |
| Enstatite + liquid = quartz + glaucophane + vapor | (Ab) |
| Liquid = albite + quartz + glaucophane + vapor | (En) |

The arrangement of these curves is presented diagrammatically in figure 7. Pure glaucophane is stable in all six fields, but for the investigated bulk composition, $Na_2O \cdot 3MgO \cdot Al_2O_3 \cdot 10SiO_2 + H_2O$, amphibole is confined to the P-T region where temperatures are less than those of curve (Q), and pressures are in excess of curve (L). Silica-saturated assemblages are indicated by heavy lines and are listed between the univariant curves.

The invariant point at 924°C and 330 bars represents the intersection of three curves indicated by the univariant reactions:

| | |
|---|---|
| Quartz = tridymite | (L), (V, En, Ab) |
| Enstatite + albite + tridymite + vapor = liquid | (Q) |
| Liquid = enstatite + albite + quartz + vapor | (Tr) |

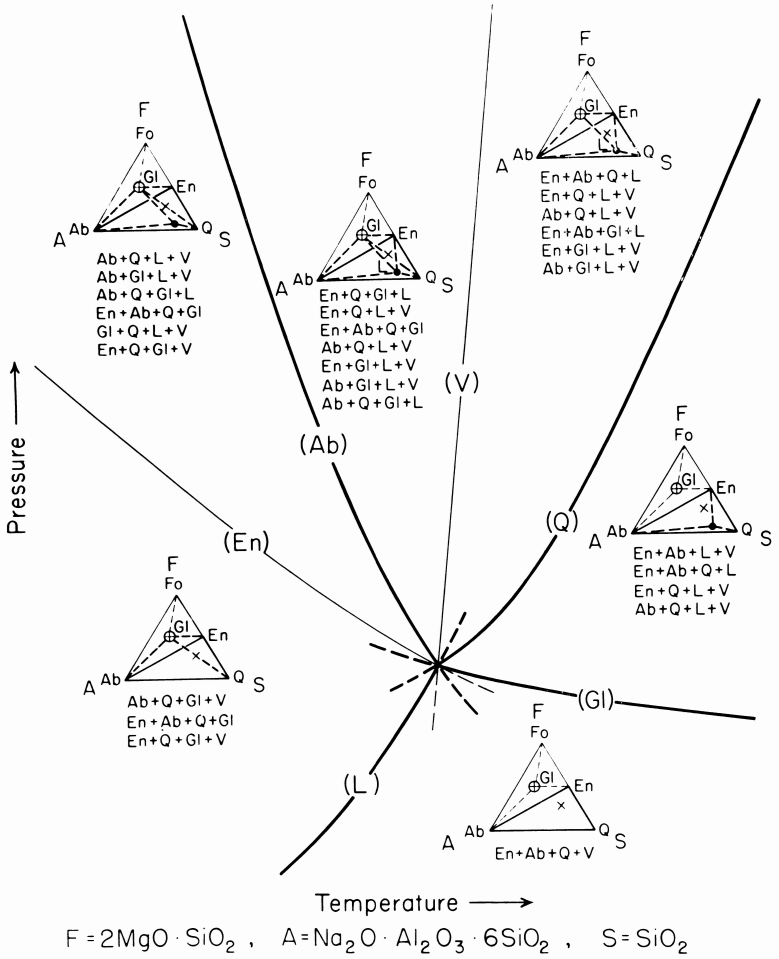


Fig. 7. Schematic arrangement of all possible curves that terminate at the invariant point at 858°C, 660 bars vapor pressure in the system $2MgO \cdot SiO_2$–$Na_2O \cdot Al_2O_3 \cdot 6SiO_2$–$SiO_2$–$H_2O$. Diagrammatic tetrahedra (in mole percent) indicate phase compatibilities between curves. Heavy joins and listed assemblages are appropriate for the subsystem supersaturated with respect to silica. Solid joins lie on the plane $2MgO \cdot SiO_2$–$Na_2O \cdot Al_2O_3 \cdot 6SiO_2$–$SiO_2$; dashed joins lie within the quaternary system $2MgO \cdot SiO_2$–$Na_2O \cdot Al_2O_3 \cdot 6SiO_2$–$SiO_2$–$H_2O$. Joins with vapor have been omitted.

This is a case of triple degeneracy (Niggli, 1954, p. 387-391), resulting from the coincidence of curves (V), (En), and (Ab) with the metastable extension of curve (L). Degeneracy occurs because one of the univariant curves (Q = Tr) is a polymorphic transition, all other phases being indifferent (Morey and Williamson, 1918). A schematic representation of these curves is presented in figure 8. As in figure 7, assemblages appropriate to the "subsystem" supersaturated with respect to silica are shown in heavy lines and are listed between the curves.

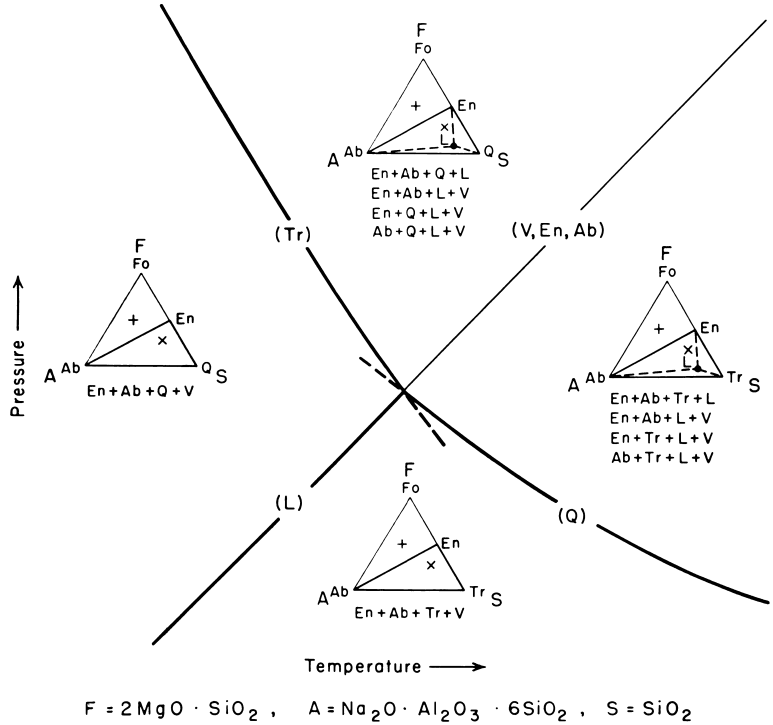


Fig. 8. Schematic arrangement of all possible curves that terminate at the degenerate invariant point at 924°C, 330 bars vapor pressure in the system $2MgO \cdot SiO_2$–$Na_2O \cdot Al_2O_3 \cdot 6SiO_2$–$SiO_2$–$H_2O$. Diagrammatic tetrahedra (in mole percent) indicate phase compatibilities between curves. Heavy joins and listed assemblages are appropriate for the subsystem supersaturated with respect to silica. Solid joins lie on the plane $2MgO \cdot SiO_2$–$Na_2O \cdot Al_2O_3 \cdot 6SiO_2$–$SiO_2$; dashed joins lie within the quaternary system $2MgO \cdot SiO_2$–$Na_2O \cdot Al_2O_3 \cdot 6SiO_2$–$SiO_2$–$H_2O$. Joins with vapor have been omitted.

### *Discussion of the Primary Crystallization Field of Glaucophane*

Treatment of the non-degenerate invariant points (figs. 6 and 7) yields information concerning glaucophane primary crystallization field boundaries diagrammatically illustrated in figure 5c. For the bulk compositions $Na_2O \cdot 3MgO \cdot Al_2O_3 \cdot 8SiO_2$ + excess $H_2O$ and $Na_2O \cdot 3MgO \cdot Al_2O_3 \cdot 10SiO_2$ + excess $H_2O$, glaucophane + liquid + vapor can coexist with either albite or enstatite, but not both; hence the primary crystallization field of glaucophane must lie between those of the other two phases. Glaucophane first appears on the liquidus surface at the quaternary minimum (point B″ in fig. 4) at 857°C and 660 bars $P_{vapor}$, and its primary field of crystallization expands with increased pressure until at 867°C and 1500 bars $P_{vapor}$ it reaches the composition of the quaternary reaction liquid (point A″ in fig. 3). At higher vapor pressures, say 2000 bars, the field boundary between forsterite and glaucophane must decline in temperature proceeding from the junction with the primary field of crystallization of enstatite (point D in fig. 5c) towards albite. This situation is indicated in figure 6 by curves (En) and (Ab); the former, along which the

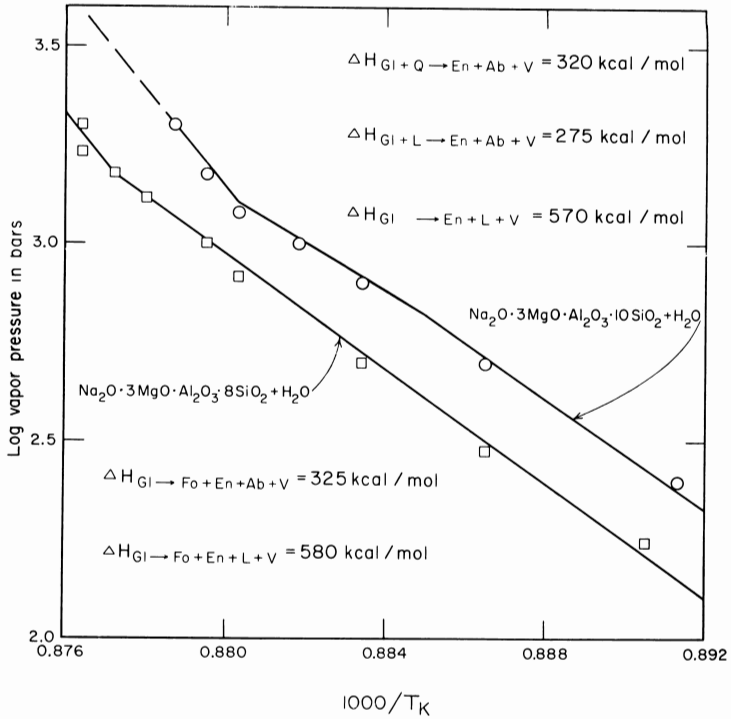


Fig. 9. Stability field of glaucophane plotted against log $P_{vapor}$ and $1/T_K$. Squares indicate curve locations for the bulk composition $Na_2O \cdot 3MgO \cdot Al_2O_3 \cdot 8SiO_2$ + excess $H_2O$; circles indicate curve locations for the bulk composition $Na_2O \cdot 3MgO \cdot Al_2O_3 \cdot 10SiO_2$ + excess $H_2O$.

phases forsterite + albite + glaucophane + liquid + vapor coexist, lies at a lower temperature than the latter, along which forsterite + enstatite + glaucophane + liquid + vapor are stable. The temperatures of the field boundaries between enstatite and glaucophane, and between albite and glaucophane must diminish towards the $SiO_2$ apex, as shown by the experimental results. The field boundary between quartz and glaucophane must decrease in temperature from the primary crystallization field of enstatite (point I in fig. 5c) towards the $Na_2O \cdot Al_2O_3 \cdot 6SiO_2$–$SiO_2$–$H_2O$ side face as indicated by fig. 7: glaucophane + liquid + vapor coexist with albite at temperatures as low as curve (En), although at higher temperatures glaucophane + liquid + vapor is in stable equilibrium with enstatite only above curve (Ab).

### *ΔH and ΔS for Reactions Involving Glaucophane*

*Glaucophane + vapor.*—The decomposition curve of a volatile-bearing mineral may closely approach a straight line plotted against log $P_{vapor}$ and $1/T_K$; the slope of this line is $-\frac{\Delta H}{2.303R}$, where R is the universal gas constant. Such treatment assumes that the vapor behaves as an ideal gas, the heat of the reaction is independent of temperature, and the volume change of reacting

condensed phases is negligible. Curves bounding the glaucophane stability field plotted against log $P_{vapor}$ and $1/T_K$, and derived values of $\Delta H$ are presented in figure 9. Dehydration of glaucophane requires approximately half the heat consumed by its incongruent melting at higher pressures.

The $\Delta H$ value of 325 kilocalories per mole for the breakdown of glaucophane to forsterite, enstatite, albite, and vapor determined by this method can be checked by calculation using the Clapeyron equation. The molar volume of synthetic glaucophane was computed from unit cell dimensions determined in this study. Molar volumes for the other phases were taken from Fairbairn (1943, table 4) and Holser and Kennedy (1959). Calculated enthalpies and entropy changes for three different points on the curve Fo + En + Ab + Gl + V are:

$\Delta H = 315$ kcal/mol, $\Delta S = 275$ cal/mol/deg, at 859°C, 500 bars $P_{vapor}$;
$\Delta H = 330$ kcal/mol, $\Delta S = 290$ cal/mol/deg, at 864°C, 1000 bars $P_{vapor}$;
$\Delta H = 340$ kcal/mol, $\Delta S = 300$ cal/mol/deg, at 867°C, 1500 bars $P_{vapor}$.

In this calculation it was assumed that the volume change of the solids is independent of temperature and pressure. It should be pointed out that evaluation of $\Delta H$ by this method depends on accurate determination of the curve slope; as can be seen from figure 3, the relative pressure insensitivity of the glaucophane stability limit prohibits accurate measurement of dP/dT.

In spite of rather large limits of error, both the integrated Clausius-Clapeyron graphical solution and the Clapeyron equation yield the same heat of reaction, 330 ± 60 kcal/mol. This value is almost an order of magnitude larger than those for most silicate dehydrations (see Ernst, 1960, table 10).

The entropy of glaucophane at 864°C and 1000 bars vapor pressure, 150 ± 50 cal/mol/deg, was obtained by subtracting the entropy change for the reaction glaucophane = forsterite + enstatite + albite + vapor (290 ± 50 cal/deg/mol) from the total entropy of the assemblage forsterite + enstatite + albite + vapor. Thermochemical data and sources are listed in table 12.

The change in coordination of aluminum from octahedral in glaucophane to tetrahedral in albite can account for only a portion of the enthalpy and entropy change involved in the decomposition of glaucophane. Reasons for the extreme values reported here are not known. Small errors in curve location would introduce large changes in $\Delta H$ and $\Delta S$, but it is clear from this investigation that the entropy and enthalpy of glaucophane are unusually low compared to other silicates.

*Quartz + glaucophane + vapor.*—The addition of $SiO_2$ depresses the high-temperature stability limit of glaucophane because the Gibbs free energy of the high-temperature assemblage is lowered (reflecting the conversion of forsterite to enstatite) relative to the free energy of glaucophane (which is silica-saturated) + quartz.

Comparison of tables 10 and 11 indicates this effect is geologically insignificant, the temperature drop of the glaucophane stability limit being only 3° to 6°C. Moreover, since dP/dT slopes are practically parallel for glaucophane with and without quartz, calculated values of $\Delta H$ and $\Delta S$ for quartz + glaucophane reactions are nearly identical to those described above for pure glaucophane. For the reaction quartz + glaucophane → enstatite + albite +

TABLE 12

Entropy data and sources

| Compound | $S_{298^\circ K}$ (cal/deg/mol) | $V_{298^\circ K}$ (cc) | $\Delta S$ 1137–298°K (cal/deg/mol) | $V_{1137^\circ K}$ (cc) | $S_{1137^\circ K}$ (cal/deg/mol) |
|---|---|---|---|---|---|
| $H_2O$ (solid) | 9.4 (7) | 13.7 | — | — | — |
| " (liquid) | 16.75 (3) | 18.0 | — | — | — |
| " (vapor) | — | — | 40.25 (3)* | 87.5† | 57.0*<br>43.1† |
| MgO | 6.55 (3) | 11.2 | — | — | — |
| $MgO \cdot H_2O$ | 15.1 (1) | 24.3 | — | — | — |
| $MgO \cdot SiO_2$ | 16.22 (3) | 31.5 | 33.6 (2) | same | 49.8 |
| $2MgO \cdot SiO_2$ | 22.75 (3) | 43.8 | 48.6 (5) | same | 71.35 |
| $3MgO \cdot 4SiO_2 \cdot H_2O$ | 62.3 (6) | 131.1 | — | — | — |
| $3MgO \cdot 2SiO_2 \cdot 2H_2O$ | 56 (9) | 101 | — | — | — |
| $7MgO \cdot 8SiO_2 \cdot H_2O$ | 130 (9) | 263 | — | — | — |
| $Na_2O \cdot Al_2O_3 \cdot 6SiO_2$ | 100.4 (4) | 202 | 172.9 (4) | same | 273.3 |
| $Na_2O \cdot Al_2O_3 \cdot 4SiO_2$ | 63.8 (4) | 121.4 | — | — | — |
| $Na_2O \cdot 3MgO \cdot Al_2O_3 \cdot 8SiO_2 \cdot H_2O$ | 136 (8) | 270 | — | same | 147.5 |
| $SiO_2$ | 10.00 (3) | 22.6 | 20.07 (2) | same | 30.07 |

(1) Giaque and Archibald, 1937.
(2) Kelley, 1949.
(3) Kelley, 1950.
(4) Kelley and others, 1953.
(5) Orr, 1953.
(6) Robie, 1957.
(7) Fyfe and others, 1958, p. 31.
(8) $\Sigma S_{298}^{Fo} + S_{298}^{En} + S_{298}^{Ab} + S_{298}^{H_2O(solid)}$ and including volume correction (Fyfe and others, 1958, p. 28-34).
(9) $\Sigma S_{298}^{oxides(solid)}$ and including volume correction (Fyfe and others, 1958, p. 28-34).

* 1 atm pressure.
† 1000 bars pressure.

vapor, the integrated Clausius-Clapeyron graphical solution (fig. 9) gives a heat of reaction of 320 kcal/mol; measurement of the curve slope at 855°C and 500 bars $P_{vapor}$ yields a value of 325 kcal/mol for $\Delta H$ and 285 cal/mol/deg for $\Delta S$. These computations are consistent with values derived for pure glaucophane and with published thermochemical data; silica saturation ($Mg_2SiO_4 + SiO_2 = 2MgSiO_3$) lowers the enthalpy of the high-temperature assemblage 7 kilocalories and the entropy 6 calories relative to the low-temperature assemblage as indicated in table 12.

### DISCUSSION OF THE LOW-TEMPERATURE STABILITY LIMIT OF GLAUCOPHANE

Experiments on the composition $Na_2O \cdot 3MgO \cdot Al_2O_3 \cdot 8SiO_2$ + excess $H_2O$ indicate that glaucophane is stable at temperatures at least as low as 602°C at 2500 bars vapor pressure (table 7). A run at 377°C and 4650 bars $P_{vapor}$ yielded albite + sodic montmorillonite; at such temperatures, reaction rates are low and equilibrium may not have been attained. If glaucophane does have

a low-temperature stability limit, it is probably replaced by a more hydrous assemblage such as albite + serpentine through the reaction:

$$Na_2O \cdot 3MgO \cdot Al_2O_3 \cdot 8SiO_2 \cdot H_2O + H_2O = Na_2O \cdot Al_2O_3 \cdot 6SiO_2 + 3MgO \cdot 2SiO_2 \cdot 2H_2O.$$

At 25°C and 1 atm total pressure, the reactants constitute the small volume, small entropy assemblage (table 12). Above 100°C, due to the vaporization of water at low pressures, they have a larger total volume and entropy than albite + serpentine. It is therefore possible that at some temperatures between the serpentine dehydration curve (Bowen and Tuttle, 1949, p. 447) and the liquid-vapor transition of water there exists a P-T region of stability for albite + serpentine. This field would pinch out at high pressures because of the rapid decrease in entropy and volume of the water. Above approximately 1000 bars $P_{vapor}$, glaucophane + water constitutes the low volume as well as the low entropy assemblage for all temperatures considered. Due to its low entropy and volume the stability of glaucophane will be almost unaffected by the partial pressure of water, but that of the assemblage albite + serpentine should be strongly influenced since its presumed stability results from the large entropy and volume of $H_2O$ at low pressures. Therefore, compatibility of albite + serpentine (if possible at all) is favored by conditions in which vapor pressure approximates total pressure; a decrease in the ratio $P_{vapor}/P_{total}$ would favor expansion of the glaucophane + vapor P-T field at the expense of albite + serpentine.

The association of albitite dikes with serpentinites has been reported from glaucophane schist terrains (e.g., California, Turner, 1896, p. 380; Japan, J. Suzuki and Y. Suzuki, 1959, p. 366-368) but it is not clear if albite and serpentine are in equilibrium. An albitite dike-serpentinite contact at Chester, Massachusetts, shown the writer by D. R. Wones, U. S. Geological Survey, displays a chlorite screen between the two rock types; hence the bulk composition of the contact zone is not equivalent to that of glaucophane (and albite + serpentine). Similarly, inclusions of albite-bearing rocks in serpentinites, and ultrabasic-graywacke contacts described from California commonly exhibit nodules or a contact selvage of actinolite + talc or actinolite + chlorite (Taliaferro, 1943, p. 150-181; Brothers, 1954, p. 622). In summary, although entropy-volume relations suggest the *possibility* of a $P_{vapor}$-T stability field for the assemblage albite + serpentine, neither experimental nor field data have yielded positive evidence of such a compatibility.

Laboratory investigation on the composition $Na_2O \cdot 3MgO \cdot Al_2O_3 \cdot 10iSO_2$ + excess water indicates that glaucophane can coexist with quartz at temperatures at least as low as 702°C at 2020 bars vapor pressure (table 8). Assemblages of equivalent bulk composition, talc + albite and anthophyllite + albite + vapor are related to quartz + glaucophane by the reactions:

$$2SiO_2 + Na_2O \cdot 3MgO \cdot Al_2O_3 \cdot 8SiO_2 \cdot H_2O = 3MgO \cdot 4SiO_2 \cdot H_2O + Na_2O \cdot Al_2O_3 \cdot 6SiO_2$$

and

$$10SiO_2 + 7(Na_2O \cdot 3MgO \cdot Al_2O_3 \cdot 8SiO_2 \cdot H_2O) = 3(7MgO \cdot 8SiO_2 \cdot H_2O) + 7(Na_2O \cdot Al_2O_3 \cdot 6SiO_2) + 4H_2O.$$

The left side of each expression constitutes the small volume, small entropy

assemblage (table 12) and should be stable at low temperatures. Inasmuch as quartz and glaucophane are in equilibrium at high temperatures as well, as indicated by the experimental investigation, albite should be incompatible with either talc or anthophyllite.

Rabbitt (1948, table 13) has listed a number of assemblages where anthophyllite is associated with sodic plagioclase, and Stillwell and Edwards (1951) have described an occurrence of talc with albite in South Australia. These associations are puzzling but they are rare compared to the abundantly described and well-documented quartz + glaucophane assemblages typical of certain low-grade metagraywackes and metacherts (e.g., California, Taliaferro, 1943; Bloxam, 1959; Japan, Suzuki, 1930).

## GEOLOGIC APPLICATION

Neither high pressure nor differential stress is required for the stable existence of glaucophane. Under appropriate chemical conditions, glaucophane is stable at magmatic temperatures; however, its absence as a primary constituent of igneous rocks attests to the fact that magmas do not satisfy such chemical requirements. By analogy with the experimentally investigated bulk compositions, $Na_2O \cdot 3MgO \cdot Al_2O_3 \cdot 8SiO_2 + H_2O$, and $Na_2O \cdot 3MgO \cdot Al_2O_3 \cdot 10SiO_2 + H_2O$, glaucophane should be stable over a wide P-T range in lime-deficient rocks which are rich in soda and magnesia relative to alumina; moreover, the presence of $Na_2O$ in excess of $Al_2O_3$ in some rocks should favor crystallization of intermediate members of the glaucophane-riebeckite series (crossites). Because of the scarcity of such chemical environments, occurrences of glaucophane over a wide range of physical conditions are rare. Possible examples of low-grade glaucophane- and crossite-bearing rocks of unusual bulk composition are presented in table 13. Chemically these rocks roughly correspond to spilites but are associated with glaucophane schists of more "nor-

TABLE 13

Glaucophane schists characterized by high $Na_2O$, low CaO contents

| Wt. percent | 1 | 2 | 3 | 4 |
|---|---|---|---|---|
| $SiO_2$ | 54.65 | 51.95 | 52.94 | 52.64 |
| $TiO_2$ | 2.99 | 2.67 | 2.20 | 2.11 |
| $Al_2O_3$ | 12.52 | 13.14 | 10.99 | 13.87 |
| $Fe_2O_3$ | 5.55 | 5.59 | 3.61 | 4.48 |
| FeO | 5.97 | 7.58 | 9.56 | 6.83 |
| MnO | 0.15 | 0.09 | 0.14 | 0.08 |
| MgO | 5.32 | 7.08 | 7.28 | 8.28 |
| CaO | 3.87 | 2.58 | 2.23 | 1.98 |
| $Na_2O$ | 6.30 | 5.46 | 7.08 | 6.08 |
| $K_2O$ | 0.21 | 1.01 | 1.14 | 0.99 |
| $H_2O^+$ | 2.15 | 2.36 | 2.30 | 2.53 |
| $P_2O_5$ | 0.36 | — | 0.30 | 0.24 |
| $CO_2$ | — | — | — | — |
| Total | 100.04 | 99.51 | 99.57 | 100.11 |

1 Chlorite-rich albite-crossitite from Corsica (Brouwer and Egeler, 1952, p. 34).

2 Albite-glaucophane schist from Switzerland (Niggli and others, 1930, p. 174).

3 Glaucophane schist from Switzerland (Niggli and others, 1930, p. 174).

4 Glaucophane (sericite-chlorite) schist from Switzerland (de Quervain and Friedlaender, 1942, p. 16).

mal" composition (low $Na_2O$, high CaO contents). Although high-grade glaucophane-bearing rocks of unusual bulk composition are theoretically possible, this author is unaware of any such occurrences.

Many glaucophane schists have compositions indistinguishable from typical greenschists and epidote amphibolites. Provided they represent equilibrium assemblages, these glaucophane schists must have formed under P-T conditions different from those of greenschists and epidote amphibolites of similar chemical composition. The problem of the glaucophane schist facies will be discussed more fully in a forthcoming paper.

ACKNOWLEDGMENTS

The author is especially indebted to F. R. Boyd, who suggested the problem, and to J. F. Schairer and H. S. Yoder, who supplied preliminary data on the system $2MgO \cdot SiO_2$–$Na_2O \cdot Al_2O_3 \cdot 6SiO_2$–$SiO_2$, all of the Geophysical Laboratory. The constructive criticisms of Boyd, Yoder, and H. P. Eugster and A. C. Waters, the Johns Hopkins University, are greatly appreciated.

Financial support of the investigation was obtained through fellowships from the Geophysical Laboratory, the National Science Foundation, and the Johns Hopkins University. The expense of five weeks of field work in California was borne by the Geophysical Laboratory.

REFERENCES

Ames, L. L., and Sand, L. B., 1958, Factors effecting maximum hydrothermal stability in montmorillonites: Am. Mineralogist, v. 43, p. 641-648.

Bloxam, T. W., 1959, Glaucophane-schists and associated rocks near Valley Ford, California: Am. Jour. Sci., v. 257, p. 95-112.

Bowen, N. L., and Tuttle, O. F., 1949, The system MgO–$SiO_2$–$H_2O$: Geol. Soc. America Bull., v. 60, p. 439-460.

Brothers, R. N., 1954, Glaucophane schists from the North Berkeley Hills, California: Am. Jour. Sci., v. 252, p. 614-626.

Brouwer, H. A., and Egeler, C. G., 1952, The glaucophane facies metamorphism in the schistes lustrés nappe of Corsica: Koninkl. Nederlandse Akad. Wetensch. Verh., Afd. Natuurk., v. 48, no. 3, 71 p.

Ernst, W. G., 1959, Alkali amphiboles: Carnegie Inst. Washington Year Book 58, p. 121-126.

———— 1960, The stability relations of magnesioriebeckite: Geochim. et Cosmochim. Acta, v. 19, p. 10-40.

Fairbairn, H. W., 1943, Packing in ionic minerals: Geol. Soc. America Bull., v. 54, p. 1305-1379.

Fyfe, W. S., Turner, F. J., and Verhoogen, Jean, 1958, Metamorphic reactions and metamorphic facies: Geol. Soc. America Mem. 73, 259 p.

Giaque, W. F., and Archibald, R. C., 1937, The entropy of water from third law of thermodynamics. The dissociation pressure and calorimetric heat of the reaction $Mg(OH)_2$ + MgO from 20°-300°K: Am. Chem. Soc. Jour., v. 59, p. 561.

Holser, W. T., and Kennedy, G. C., 1959, Properties of water. Part V. Pressure-volume-temperature relations of water in the range 400-1000°C and 100-1400 bars: Am. Jour. Sci., v. 257, p. 71-77.

Kelley, K. K., 1949, Contributions to the data on theoretical metallurgy. X. High-temperature heat content, heat capacity and entropy data for inorganic compounds: U. S. Bur. Mines Bull. 476, 241 p.

———— 1950, Contributions to the data on theoretical metallurgy. XI. Entropies of inorganic substances: U. S. Bur. Mines Bull. 477, 147 p.

Kelley, K. K., Todd, S. S., Orr, R. L., King, E. G., and Bonnickson, K. R., 1953, Thermodynamic properties of sodium-aluminum and potassium-aluminum silicates: U. S. Bur. Mines Rept. Inv. 4955, 21 p.

Kunitz, W., 1930, Die Isomorphieverhaeltnisse in der Hornblendegruppe: Neues Jahrb. Mineralogie, Geologie u. Paläontologie Beilage-Band 60, Abt. A., p. 171-250.

Morey, G. W., and Williamson, E. D., 1918, Pressure-temperature curves in univariant systems: Am. Chem. Soc. Jour., v. 40, p. 59-84.

Nagelschmidt, G., 1938, On the atomic arrangement of the members of the montmorillonite group: Mineralog. Mag., v. 25, p. 140-155.

Niggli, Paul, 1954, Rocks and mineral deposits: San Francisco, W. H. Freeman and Co., 559 p.

Niggli, Park, Quervain, Francis de, and Winterhalter, R. V., 1930, Chemismus schweizerischer Gesteine: Schweiz. geol. Beitr., Geotech. Ser., Lief. 16, 389 p.

Orr, R. L., 1953, High-temperature heat contents of magnesium orthosilicate and ferrous orthosilicate: Am. Chem. Soc. Jour., v. 75, p. 528-529.

Quervain, Francis de, and Friedlaender, Carl, 1942, Nachrag zu "Chemismus schweizerischer Gesteine": Schweiz. geol. Beitr., Geotech. Ser., Lief. 20, 108 p.

Rabbitt, J. C., 1948, A new study of the anthophyllite series: Am. Mineralogist, v. 33, p. 263-323.

Robie, R. A., 1957, Thermodynamic properties of $CaMg(CO_3)_2$, $Mg_3Si_4O_{10}(OH)_2$, and $Ca_2Mg_5Si_8O_{22}(OH)_2$ between 1200 and 300°K: Unpub. Ph.D. thesis, Univ. Chicago, 107 p.

Schairer, J. F., and Yoder, H. S., 1960, The ternary system $Na_2O \cdot Al_2O_3 \cdot 6SiO_2$–$2MgO \cdot SiO_2$–$SiO_2$: Carnegie Inst. Washington Year Book 59, p. 69-70.

Stillwell, F. L., and Edwards, A. B., 1951, Petrology of the Gumeracha talc deposits: Geol. Soc. South Australia Bull. 26, p. 31-49.

Suzuki, J., 1930, Petrological study of the crystalline schist system of Shikoku, Japan: Hokkaido Imp. Univ., Fac. Sci., Jour., ser. IV, v. 1, p. 27-111.

Suzuki, J., and Suzuki, Y., 1959, Petrological study of the Kamuikotan metamorphic complex in Hokkaido, Japan: Hokkaido Univ., Fac. Sci., Jour., ser. IV, v. 10, p. 349-446.

Taliaferro, N. L., 1943, Franciscan-Knoxville problem: Am. Assoc. Petroleum Geologists Bull., v. 27, p. 109-219.

Turner, H. W., 1896, Notice of some syenitic rocks from California: Am. Geologist, v. 17, p. 375-388.

Tuttle, O. F., and Bowen, N. L., 1958, Origin of granite in the light of experimental studies in the system $NaAlSi_3O_8$–$KAlSi_3O_8$–$SiO_2$–$H_2O$: Geol. Soc. America Mem. 74, 153 p.

Tuttle, O. F., and England, J. L., 1955, Preliminary report on the system $SiO_2$–$H_2O$: Geol. Soc. America Bull., v. 66, p. 149-152.

Winchell, A. N., and Winchell, H., 1951, Elements of optical mineralogy. Part II. Descriptions of minerals: New York, John Wiley and Sons, Inc., 551 p.